



Slovak Biophysical Symposium

Book of Contributions

Herľany
March 26 – 29, 2006

Editors
FABRICOVÁ Gabriela
MIŠKOVSKÝ Pavol

Organisers

Slovak Biophysical Society

&

Department of Biophysics
Faculty of Science, P. J. Šafárik University

Program Committee

CHORVÁT Dušan
HIANIK Tibor
JAKUŠ Ján
MIŠKOVSKÝ Pavol

Organising Committee

BÁLINT Štefan
FABRICOVÁ Gabriela
GBUR Peter
LAJOŠ Gejza
MIŠKOVSKÝ Pavol
NAĐOVÁ Zuzana
STEHLÍKOVÁ Mária

Chairman

MIŠKOVSKÝ Pavol

Address

Department of Biophysics
Faculty of Science
University of P. J. Šafárik
Jesenná 5
041 54 Košice

Tel:+421 55 622 19 26

Conference e-mail

sbs@seneca.science.upjs.sk

Conference web site

<http://seneca.science.upjs.sk/~sbs/>

CONTENTS

PROGRAM

MONDAY, MARCH 27	9
TUESDAY, MARCH 28	11
WEDNESDAY, MARCH 29	12

ABSTRACTS

PLENARY LECTURES	15
LECTURES	17
MONDAY	17
TUESDAY	29
WEDNESDAY	33
POSTER SESSION	45
LIST OF PARTICIPANTS	75
AUTHOR INDEX	81



PROGRAM

7:30-8:30

BREAKFAST

8:45-9:00

OPENING

Chairmann: P. Miškovský

9:00-10:00

PLENARY LECTURE

Mechanisms of protein-DNA interactions at surfaces

T. HIANIK

10:00-10:30

COFFEE BREAK

10:30-11:30

PLENARY LECTURE

Fluorescence spectroscopy and imaging

D. CHORVÁT, JR.

12:00-13:00

LUNCH

Chairmann: T. Hianik

13:00-13:20

LECTURE

Basic quantitative methods of EEG data analysis

P. MURÍŇ

13:25-13:45

LECTURE

Allosteric gating of ryanodine receptor

A. ZAHRADNÍKOVÁ

13:50-14:10

LECTURE

Kinetics of calcium current inactivation is locally controlled by calcium release

I. ZAHRADNÍK

14:15-14:35

LECTURE

Automating conventional patch-clamp and lipid bolayer experiments

P. NOVÁK

MONDAY, MARCH 27

14:40-15:00

COFFEE BREAK

Chairmann: J. Uličný

15:00-15:20

LECTURE

Kinetics of reduction of the catalytic site in mitochondrial cytochrome c oxidase

D. JANCURA

15:25-15:45

LECTURE

Photogeneration of singlet oxygen by hypericin in complexes with low density lipoproteins: An infrared phosphorescence study

P. GBUR

15:50-16:10

LECTURE

Optical spectra of photoactive drug naphthazarin in solutions

M. SAVKO

17:00-18:00

MEETING OF SLOVAK BIOPHYSICAL SOCIETY

18:30-

CONFERENCE RECEPTION

7:30-8:30

BREAKFAST

Chairmann: D. Chorvát, jr.

9:00-10:00

PLENARY LECTURE

Raman spectroscopy and imaging

P. MIŠKOVSKÝ

10:00-10:30

COFFEE BREAK

10:30-11:30

PLENARY LECTURE

From molecular simulations to predictive modelling

J. ULIČNÝ

12:00-13:00

LUNCH

Chairmann: I. Zahradník

13:00-13:20

LECTURE

Mitochondrial redox responses in isolated rat cardiomyocytes studied by spectrally and spatially resolved flavin fluorescence

J. KIRCHNEROVÁ

13:25-13:45

LECTURE

Study of resorcin[4]arene-dopamine complexation in mixed phospholipid monolayers

P. VITOVÍČ

13:50-14:00

COFFEE BREAK

14:00-15:00

POSTER SESSION

15:30-

EXCURSION TO VINIČKY (TOKAJ WINE REGION)

7:30-8:30

BREAKFAST

Chairmann: D. Jancura

9:00-9:20

LECTURE

Comparison of thermodynamic properties of release factors 2 from Escherichia coli and Thermus thermophilus

E. SEDLÁK

9:25-9:45

LECTURE

Amino acid propensities for flavin adenine dinucleotide binding sites in proteins

K. TÓTH

9:50-10:10

LECTURE

Dynamics of active site of NADH oxidase from Thermus thermophilus: experiments and molecular dynamics

E. SEDLÁK

10:15-10:35

COFFEE BREAK

Chairmann: A. Zahradníková

10:35-10:55

LECTURE

Imaging of polymer distribution in polyelectrolyte microcapsules using covalently bound fluorescent markers and confocal laser scanning microscopy

J. PODSKOČOVÁ

11:00-11:20

LECTURE

Estimation of single cardiomyocyte volume by active countour algorithm

M. CAGALINEC

11:25-11:45

LECTURE

Photodynamic therapy of gastrointestinal superficial polyps with aminolevulinic acid. A clinical and spectroscopic study

J. SMOLKA

11:50-12:00

CLOSING OF SLOVAK BIOPHYSICAL SYMPOSIUM

12:00-13:00

LUNCH



ABSTRACTS

Mechanisms of protein-DNA interactions at surfaces

T. HIANIK¹, I. GRMAN¹ AND M. THOMPSON²

¹Department of Nuclear Physics and Biophysics, FMFI UK, Mlynská dolina F1, 842 48 Bratislava, Slovakia

²Department of Chemistry, University of Toronto, 80 St. George Street, Toronto, Ontario M5S 3H6 Canada

e-mail: hianik@fmph.uniba.sk

The protein-DNA interactions are of great biological significance. They are responsible for transcription of DNA, gene expression as well as for formation of specific structures of chromosomes and viruses [1]. The practical interest in the study of the mechanisms of protein-DNA interactions is connected also with a new direction in biosensing, based on aptamers – the specific sequences of DNA or RNA that can recognize the proteins with a high specificity [2,3]. In this contribution we report short overview on current knowledge on the mechanisms of protein-DNA interaction with focus on these interaction at surfaces. Using the thickness shear mode method (TSM) we studied the interaction of thrombin with DNA aptamers immobilized on a thin gold layer covered the AT-cut quartz. The thickness-shear mode (TSM) acoustic method is highly sensitive tool for on-line detection of binding events at the surfaces. It is based on application of electric field to AT-cut quartz crystal through electrodes and as a results the generation of acoustic shear wave in a thickness direction took place. The sensing layer is placed at one side of the crystal. The shear wave propagates through the film and into the liquid and can be characterized from the storage and dissipation processes. The measured electrical impedance of the sensor is related to complex acoustic impedance. As a result series resonance frequency f_s and motional resistance R_m is determined. The value of f_s represent the energy storage and reflects the mass changes of the oscillating layer, while R_m is related to energy dissipation and evidence on changes of shearing viscosity of the layer [4]. We immobilized biotinylated 32 mer DNA aptamer specific to thrombin onto a 9 MHz AT-cut quartz covered by neutravidin. Using a network analyzer HP4395A the impedance properties of the layer were studied. We showed, that interaction of the thrombin with aptamer resulted in decrease of the f_s value, while motional resistance increases. The decrease of f_s due to binding process is well known phenomena and is connected with increase of the mass of the crystal. The increase of the R_m value suggests on the increase of viscosity forces. Certainly, without thrombin the aptamers immobilized on a quartz surface are partly in unfolded and partially in folded conformation. Addition of the thrombin resulted in shift of the equilibrium to a folded aptamer conformation and in increase of the thickness of the layer. This resulted in increase of the friction between the layer and the surrounding solvent (buffer). We showed, that sodium ions in a concentration range 0-500 mM have substantial effect on the binding affinity of thrombin to the aptamer. For all Na^+ concentrations the f_s value decreases with increasing thrombin concentration. The effect of the changes of f_s is, however maximal at 10 mM NaCl, while minimal at highest ionic strength (500 mM). When no Na^+ ions are present the changes of f_s are intermediate between 10 and 50 mM NaCl. It is likely that effect of Na^+ ions is connected with screening of negative charges of DNA aptamers and thus decreasing the affinity of positively charged thrombin to its DNA binding site. On the other hand, lower binding affinity of thrombin without Na^+ ions in comparison with 10 mM NaCl revealed, that sodium ions together with potassium ions (K^+ ions were always present in a buffer) are necessary for maintaining three dimensional structure of the aptamers [5].

Acknowledgement

This work was supported by the research grant from the Slovak Grant Agency Vega No. 1/1015/04, by Agency for Promotion Research and Development under the contract No. APVV-20-P01705, by the NATO SfP Program (Project No. SfP – 978003), by European Commission (Project No. FOOD-CT-2004-506579) and Ministry of Education of Slovak Republic.

References

- [1] S. Neidle, *Nucleic Acid Structure and Recognition*, Oxford University Press, Oxford (2002).
- [2] S. Tombelli, M. Minunni and M. Mascini, *Biosens. Bioelectr.* 20 (2005) 2424-2434
- [3] T. Hianik, V. Ostatná, Z. Zajacová, E. Stoikova and G. Evtugyn, *Bioorg. Med. Chem. Lett.* 15 (2005) 291-295.
- [4] J.S. Ellis and M. Thompson, *Phys. Chem. Chem. Phys.* 6 (2004) 4928-4938.
- [5] B.I. Kankia and L.A. Marky, *J. Am. Chem. Soc.* 123 (2001) 10799-10804.

Basic quantitative methods of EEG data analysis

P. MURÍN¹, J. JAKUŠ¹ AND E. KURČA²

¹ Institute of Medical Biophysics, Comenius University, Jessenius Faculty of Medicine, Malá hora 4, 037 54 Martin, Slovakia

² Clinic of Neurology, Faculty Hospital in Martin, Kollárova 2, 036 59 Martin, Slovakia
e-mail: pmurin@jfmed.uniba.sk

Nowadays almost each electroencephalographic (EEG) workplace is equipped with a digital EEG. So the techniques of quantitative EEG analysis (QEEG) are becoming more available and popular. Wide spectrum of computer programs is helpful not only with fast saving, making backups and browsing the EEG-records but also with numbers of modern techniques of EEG analysis.

This study aims to overview QEEG methods of filtration, the artefacts removing, topographic brain-mapping, frequency and spectral analysis, power spectrum and coherence. The main part of study deals with new perspective method – cordance – that joins the information from absolute and relative power. Cordance is closely correlated with regional cerebral perfusion. Authors briefly present their own approach in solving of above-mentioned problems.

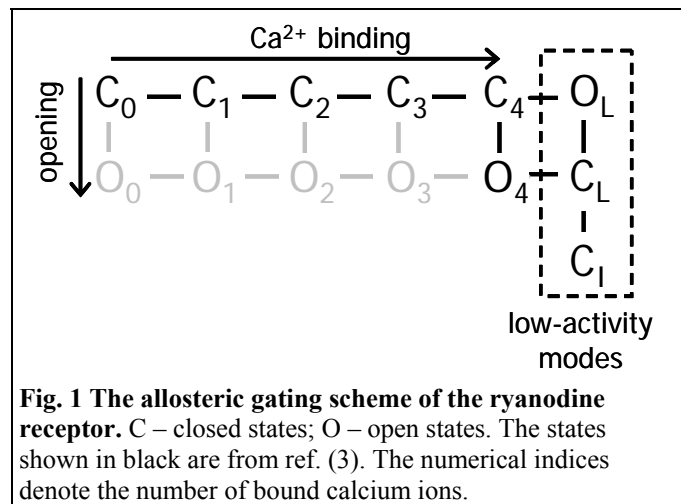
Allosteric gating of the ryanodine receptor

A. ZAHRADNÍKOVÁ AND I. ZAHRADNÍK

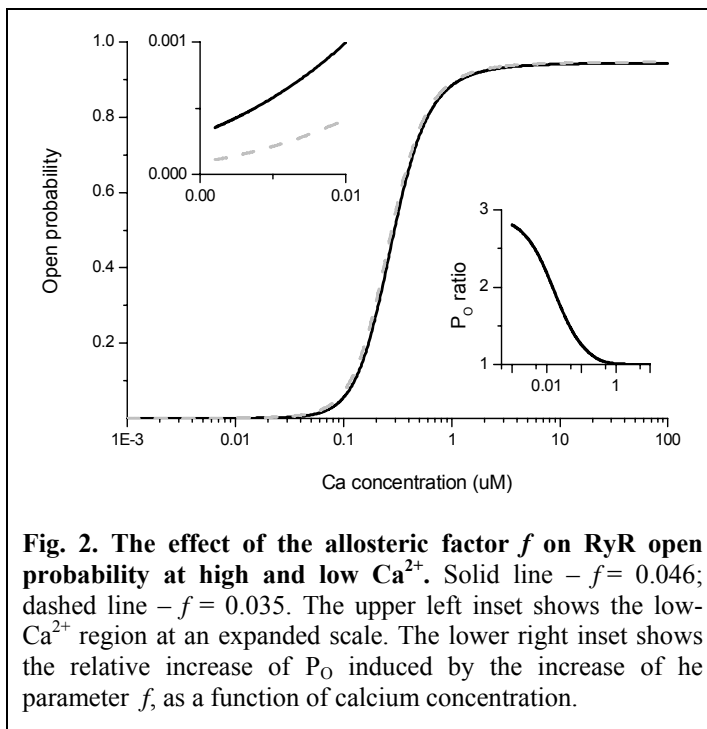
ÚMFG SAV, Vlárská 5, 833 34 Bratislava, Slovakia.
e-mail: alexandra.zahradnikova@savba.sk

Ryanodine receptors (RyRs) provide the cytoplasm of cardiac myocytes with calcium ions that are required for contraction. They open in response to local increases in calcium concentration caused by openings of the voltage-activated calcium channels on the plasma membrane, and thus release calcium stored in the sarcoplasmic reticulum. Defective regulation of calcium release has been observed in a variety of cardiac diseases (such as hypertrophy, heart failure, and the hereditary arrhythmias catecholaminergic polymorphic ventricular tachycardia and arrhythmogenic right ventricular dysplasia): calcium release in response to the electrical stimulus is decreased, calcium release in the absence of the stimulus is increased, or both. The mechanism by which the diseases affect activation of RyRs is not known.

Previously it was generally accepted that ryanodine receptors can open only after binding of (several) calcium ions. We have found that the calcium dependence of RyRs composed of both, wild-type monomers and monomer(s) deficient in calcium-dependent activation [1] cannot be adequately described by such linear models. On the other hand, the high-conductance Ca^{2+} -activated potassium channel has been shown to possess separate pathways for channel opening and for calcium binding, and its activation is understood as the result of allosteric coupling between the two processes [2]. Therefore we modified our extended minimal gating (EMG) model [3] to include allosteric coupling. We analyzed the effects of allosteric coupling, modal gating, and structure of the calcium binding site, either separately or in combination, on the calcium dependence of activation of RyR variants with variable number of mutant monomers. To adequately describe the effect of mutation on RyR activity [1], the RyR model required (i) four independent calcium binding sites, (ii) allosteric coupling between calcium binding and channel opening, and (iii) the presence of low-activity gating modes (Figure 1). In the optimal “allosteric extended minimal gating” (aEMG) model, in addition to the parameters of the EMG model, described previously [3], RyR gating is regulated by the allosteric factor f that determines the relative propensity of the channel to open in the absence and presence of Ca^{2+} . The calcium dependences of the wild-type ryanodine receptor in the aEMG and EMG models were indistinguishable.



Simulations with varying extent of allosteric coupling between calcium binding and channel opening revealed that increasing the parameter f selectively augmented open probability at low calcium concentrations, while leaving the overall calcium dependence of RyR activity unchanged (Figure 2). The increase in open probability is significant only at calcium concentrations that evoke a very low level of open probability, and therefore they are not easily detectable in single-channel experiments. However, the size of the effect is sufficiently



high to explain the previously observed increase in the frequency of diastolic spontaneous calcium release events in inherited [4] or acquired [5] cardiac diseases.

Thus, allosteric interaction between calcium binding and channel opening can explain the variable tendency of the ryanodine receptor to activate at low levels of Ca^{2+} by changes in the allosteric factor f . Further development of the approach used in this work to determine the mechanisms underlying variation of f ; will be useful in understanding molecular mechanisms of heart failure.

Acknowledgement

This work was supported by the grants VEGA 2/4150/04, APVT-51-31104, and NIH RO3 TW005543.

References

- [1] Li P, Chen SR, *J Gen Physiol* 118: 33-44, 2001.
- [2] Cox DH, Cui J, Aldrich RW, *J Gen Physiol* 110: 257-281, 1997.
- [3] Zahradníková A, Zahradník I, Györke I, Györke S, *J Gen Physiol* 114: 787-798, 1999.
- [4] Viatchenko-Karpinski S, Terentyev D, Györke I, Terentyeva R, Volpe P, Priori SG, Napolitano C, Nori A, Williams SC, Györke S. *Circ Res* 94:471-477, 2004.
- [5] Kubalova Z, Terentyev D, Viatchenko-Karpinski S, Nishijima Y, Györke I, Terentyeva R, da Cunha DN, Sridhar A, Feldman DS, Hamlin RL, Carnes CA, Györke S. *Proc Natl Acad Sci USA* 102: 14104-14109, 2005.

Kinetics of calcium current inactivation is locally controlled by calcium release

I. ZAHRADNÍK, J. PAVELKOVÁ, A. ZAHRADNÍKOVÁ, JR., E. POLÁKOVÁ, Z. KUBALOVÁ, AND A. ZAHRADNÍKOVÁ

ÚMFG SAV, Vlárská 5, 833 34 Bratislava, Slovakia.
e-mail: ivan.zahradnik@savba.sk

Contraction of cardiac myocytes is a direct response of their contractile fibrils to transient elevation of intracellular calcium ion concentration. The time course and amplitude of calcium concentration changes are controlled by the process known as excitation-contraction (E-C) coupling. The structural substrate of this process is a specialized junction of the plasma membrane with terminal cisterns of the sarcoplasmic reticulum, termed the dyad, that represents the elementary unit of E-C coupling or the couplon [1]. Mechanistic understanding of the function of the dyad is limited by its small size, complex structure and complex physico-chemical interactions between the channels and ions involved. In this work we focus on the inactivation of the voltage dependent calcium channels (L-type calcium channels) of the plasma membrane.

It is well known that L-type calcium channels open (activate) in response to depolarizing voltage pulses and close (inactivate) in a calcium-dependent manner. Activation of these channels manifests as the calcium current (I_{Ca}) that can be recorded in isolated cardiac myocytes by the patch-clamp technique. Activation is very fast. Calcium currents peak in about 5 ms. Decline of the calcium current (inactivation) has two time components. The fast one, of about 7-ms time constant, is related to increased intracellular Ca^{2+} concentration due to release of calcium ions from terminal cisterns of the sarcoplasmic reticulum. Therefore, it is termed release-dependent inactivation (RDI). We have shown previously [2, 3], using combined measurements of calcium currents by the patch-clamp method and of calcium spikes, the intracellular calcium transients, by a confocal microscope, that RDI is controlled locally by calcium ions within the dyad and not globally by the overall increase of intracellular calcium. Here we test the hypothesis that the slow component of the calcium current inactivation is controlled by local calcium release as well, and compare it with the hypothesis that the slow component of inactivation is controlled by the calcium current itself. We employ the method of mathematical modeling, that is, approximation of the recorded calcium currents with theoretical equations derived for a specific mechanism.

$$I_{Ca}(t) = I_M \cdot P_A(t) \cdot (1 - F_R \cdot P_{RDI}(t)) \cdot (1 - F_S \cdot P_{SI}(t))$$

$$P_{RDI}(t) = \int_0^t \int_0^T pdfR(\tau) \cdot pdfI_R(T - \tau) \cdot d\tau dT$$

$$P_{CDI}(t) = \int_0^t \int_0^T pdfC(\tau) \cdot pdfI_C(T - \tau) \cdot d\tau dT$$

$$P_{DDI}(t) = \int_0^t \int_0^T pdfR_S(\tau) \cdot pdfI_{RS}(T - \tau) \cdot d\tau dT$$

$$P_{I,Ca} = 1 - e^{-k_R[Ca]t}$$

Fig. 1 Equations describing the kinetics of calcium current.

To characterize the kinetics of the release-dependent inactivation (RDI) quantitatively, we have developed two models that account for the local control of calcium release activation and for the subsequent rapid inactivation of I_{Ca} (Figure 1). Both models were based on the concept of independent excitation-contraction coupling units (couplons) and assumed that calcium current activation triggers activation of calcium release with a variable probability and that the subsequent inactivation of calcium

channels by the released calcium is immediate. The models differed in the description of the slow component of inactivation. In the CDI model, it was modeled as current-dependent

inactivation affecting all calcium channels.

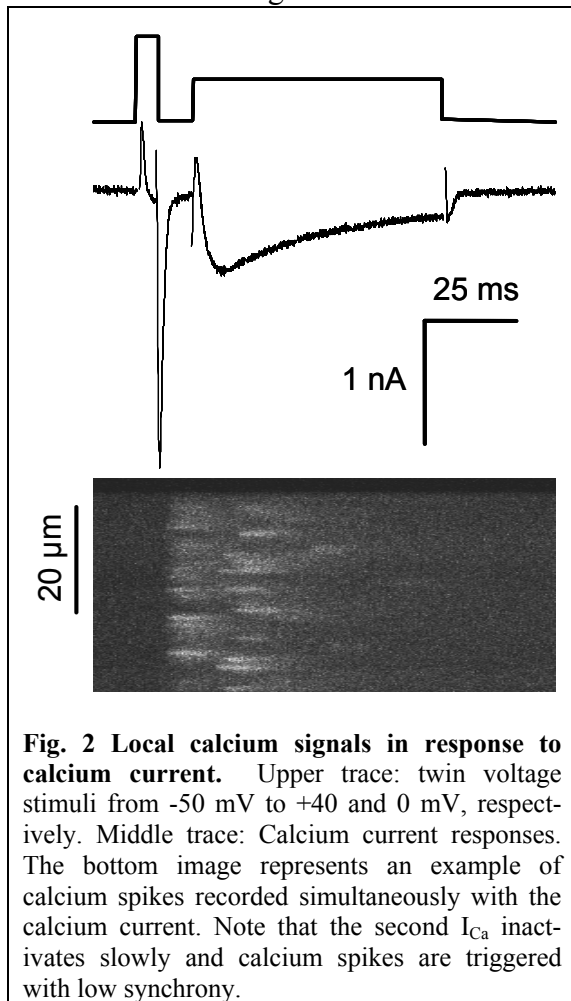


Fig. 2 Local calcium signals in response to calcium current. Upper trace: twin voltage stimuli from -50 mV to +40 and 0 mV, respectively. Middle trace: Calcium current responses. The bottom image represents an example of calcium spikes recorded simultaneously with the calcium current. Note that the second I_{Ca} inactivates slowly and calcium spikes are triggered with low synchrony.

In the DDI model, it was modeled as a process evoked by late calcium release events that affected only a fraction of channels (Figure 2). While both models provided good description of the kinetics of I_{Ca} and showed excellent convergence, the DDI model provided significantly lower χ^2 values. Both models provided the same values of parameters of I_{Ca} activation and of the fast component of RDI. The degree of RDI and the synchrony of calcium release had a bell-shaped dependence on membrane potential, while the delay between the stimulus and the maximal release had a U-shaped dependence. The probability of triggering calcium release decreased with membrane potential. The voltage dependence of RDI parameters suggests that triggering of release by I_{Ca} is controlled by the rate of calcium channel activation at negative membrane potentials while it is controlled by the unitary Ca^{2+} current amplitude at positive potentials. Once the release event in the couplon is triggered, all its adjoined calcium channels inactivate. The duration of the delay between activation of calcium current and activation of calcium release suggests that the fidelity of coupling between DHPR and RyR channels is substantially less than one at all membrane potentials. The new kinetic model of calcium

current provides means to track Ca^{2+} release in situ under physiological conditions.

Acknowledgement

This work was supported by the grants VEGA 2/4153/04, APVT-51-31104, and NIH RO3 TW005543.

References

- [1] Stern MD, Song LS, Cheng H, Sham JS, Yang HT, Boheler KR, Rios E. *J Gen Physiol* Mar;113: 469-489, 1999.
- [2] Zahradnikova A, Kubalova Z, Pavelkova J, Gyorke S, Zahradnik I. *Am J Physiol Cell Physiol* 286: C330-341, 2004.
- [3] Zahradnikova A, jr., Polakova E, Zahradnikova A, Zahradnik I. *FASEB J* 19: A559, 2005.

Automating conventional patch – clamp and lipid bilayer experiments

P. NOVÁK AND I. ZAHRADNÍK

Institute of Molecular Physiology and Genetics, Slovak Academy of Sciences, Vlárská 5, 833 34 Bratislava, Slovakia.

e-mail: pavel.novak@savba.sk

Introduction of the patch-clamp technique twenty-five years ago [1] revolutionized the field of cellular electrophysiology and defined a new standard for high-resolution measurement of electrical properties of membranes and ion channels. In recent years, the instrumentation of the patch-clamp method itself has undergone a new revolution in order to eliminate its low-throughput and high demands on training and technical skills. A number of recently developed commercial automated patch-clamping systems utilize either a completely new planar-electrode technology or modified glass-pipette technology (for a review see [2]). Most of these systems are designed primarily as high-throughput screening tools for drug development, while researchers working on more complex preparations such as brain slices or freshly isolated myocytes still have to rely on the conventional labor-intensive patch-clamp methodology. However, also for conventional patch-clamp approach many routines and operations can be automated, since typical patch-clamp set-ups includes a personal computer, digitizer with multiple inputs and outputs and other devices for external control of analog or digital devices (electronic micromanipulator, perfusion system, pipette pressure system etc.). Unfortunately, there's little support for automation in available software tools for the basic-research oriented patch-clamp experiments. The situation is very similar in the case of single channel experiments with planar lipid membranes (PLM). PLM experiments are supported by many patch-clamp amplifiers as an alternative to the patch-clamp technique, however, a handy software tool for monitoring formation of bilayers is missing.

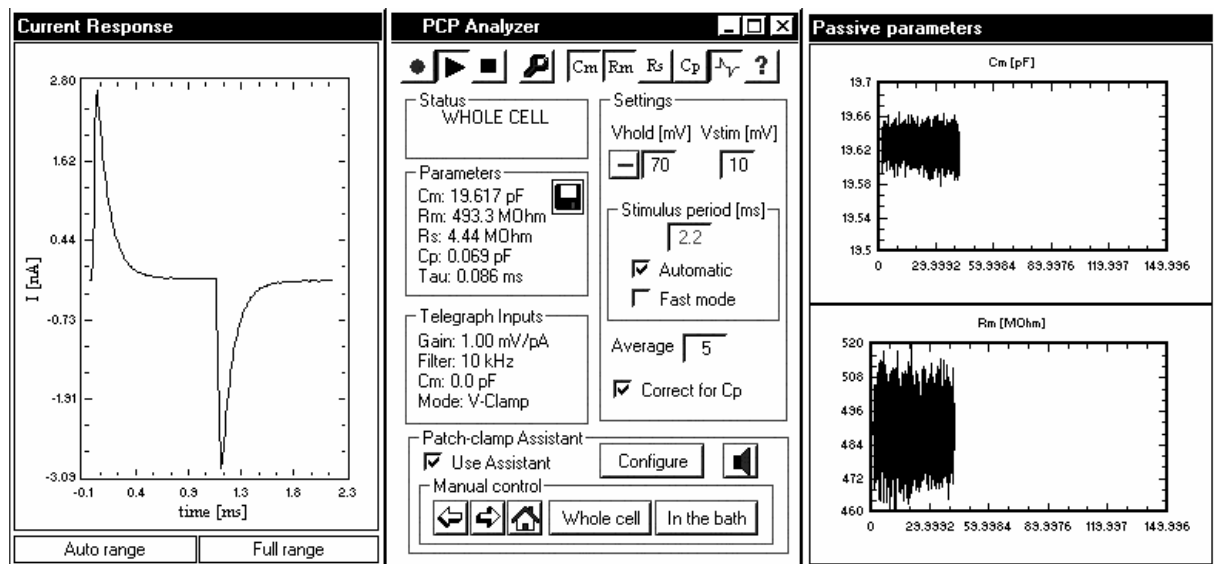


Fig. 1 PCP Analyzer for assistance in measurements of electrical properties during conventional patch-clamp experiments.

The ability to automate basic tasks of patch-clamp or PLM experiments is directly linked to the recognition of the actual current measurement configuration or state. In the present study we focused on development of the software state automaton for automatic

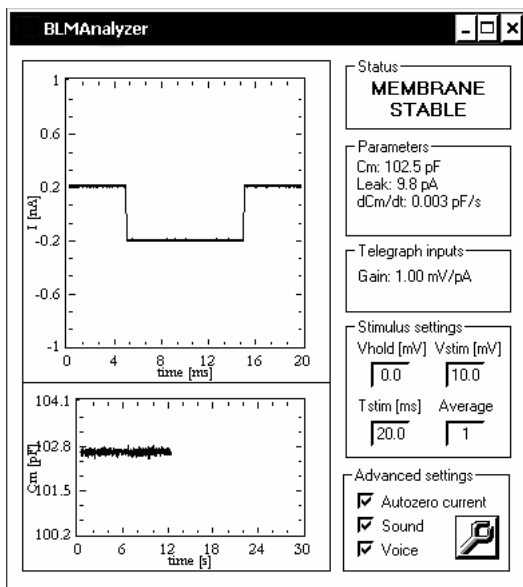


Fig. 2 BLM Analyzer for monitoring of planar lipid membrane formation.

recognition of current recording state during formation of the whole-cell patch-clamp configuration. The process of whole-cell state formation was represented by five working states (“In Air”, “In Bath”, “On Cell”, “Gigaseal” and “Whole-cell”) and three error states (“Broken pipette”, “Lost Seal” and “Lost Cell”). Transitions between the states are determined by the shape of current response to the square wave voltage stimulation and values of resistive parts of impedance estimated from current response. Shape of current response is evaluated by means of the ratio between charges measured within specific time segments of current response. Measured charges are simultaneously used for calculation of pipette or seal resistance prior to whole-cell formation and for high-resolution measurement of membrane capacitance, membrane resistance and access resistance in the whole-cell configuration. In case of PLM

experiments, the whole process of bilayer formation was represented by three states: “No Membrane”, “Membrane Formation” and “Membrane Stable”. Transitions between states are determined by the shape of the current response to a triangle wave voltage stimulus, leak current value and membrane capacitance trend utilizing charge evaluation in a way similar to the patch-clamp technique.

State automatons for assistance during patch-clamp and PLM experiments were implemented separately in two software tools PCP Analyzer (Fig.1) and BLM Analyzer (Fig.2), both adapted to Digidata 132X family of data-acquisition systems (Axon Instruments, USA). Based on the currently recognized state of patch-clamp experiment, the PCP Analyzer is able to choose automatically the proper set of measured parameters, to set predefined amplitude and holding potential of square wave voltage stimulus, to adjust stimulation frequency for optimal resolution, to issue sound alerts and to control external devices such as the z-drive of the micromanipulator or the patch-pipette pressure system. Important information about the process of the whole-cell formation is saved day by day in a separate log file for later reference. The BLM Analyzer uses sound alerts and synthesized voice to notify the experimenter that a membrane started to form in the aperture of the measurement chamber or that the thinning process of bilayer has finished and the membrane is stable. In addition to automatic setting of predefined values of holding voltage and stimulus amplitude according to the currently recognized state, the BLM Analyzer offers automatic zeroing of the leak current prior to the formation of the membrane.

Both tools were appreciated by newcomers mastering the patch-clamp or PLM techniques as well as by skilled scientists looking for smart software tools that would simplify the single channel or whole-cell current recordings or membrane capacitance measurement.

Acknowledgement

This work was supported by VEGA 2/4153/24.

References

- [1] O. P. Hamill, A. Marty, E. Neher, B. Sakmann and F. J. Sigworth, *Pflügers Arch.* 391 (1981), 85-100.
- [2] X. Wang, M. Li, *Assay Drug Dev. Technol.* 1 (2003), 1 – 13.

Kinetics of reduction of the catalytic site in mitochondrial cytochrome *c* oxidase

D. JANCURA¹, M. ANTALÍK², V. BERKA³, G. PALMER⁴ AND M. FABIÁN⁴

¹ Department of Biophysics, Safarik University, Kosice

² Biophysical Laboratory, Institute of Experimental Physics, Kosice

³ Department of Internal Medicine, University of Texas, Health Science Center, Houston, TX

⁴Department of Biochemistry and Cell Biology, Rice University, Houston, TX

Mitochondrial cytochrome *c* oxidase (CcO) is a membrane protein that catalyzes the oxidation of ferrocytochrome *c* (cyt c^{2+}) by molecular oxygen. The reduction of oxygen to water requires the delivery of four electrons and four protons into the catalytic center of the enzyme. Electrons enter oxidase from the cytosolic domain and protons from the matrix side of the inner mitochondrial membrane. This redox reaction is coupled to the pumping of four additional protons across the membrane. Both of these processes contribute to the generation of a transmembrane proton gradient.

Bovine heart CcO contains 13 polypeptides and four redox centers that are involved in electron transport (ET) and in the reduction of O₂ to water. Three of these centers, heme *a*, heme *a*₃ and copper ion, called Cu_B, are in subunit I and the dinuclear copper center, Cu_A, is located in subunit II [1]. Cu_A is close to the cytosolic surface of the protein and serves as the acceptor of electrons either from the physiological reductant, cyt c^{2+} , or artificial electron donors. Electrons received by the oxidase are rapidly distributed between Cu_A and heme *a* on the microsecond timescale. ET continues further to the catalytic center composed of heme *a*₃ and Cu_B. At this catalytic center, the interaction of electrons, protons and oxygen occurs [for reviews see 2-4].

The catalytic center is buried within the protein, and the chemical reactions are therefore dependent on pathways or channels which facilitate proton and oxygen diffusion to the active site. Two plausible proton-conducting pathways, named the D- and K-channels, because of highly conserved Asp91 and Lys319, respectively, have been identified [1]. These two pathways connect the catalytic site with the mitochondrial matrix phase

The reaction of CcO with oxygen can be realized only when the catalytic center is fully reduced. The transfer of two electrons to the oxidized catalytic center, which is necessary for the full reduction of this center, is accompanied with uptake of two protons, ultimately from solution [5,6]. The rate of heme *a*₃ reduction appears to be simultaneous with proton uptake and it has been concluded that the rate limiting process for this internal ET is the stabilization of the electrons by protons [7,8].

In this study, combination of EPR spectroscopy, the rapid-freeze method and the stopped-flow method was used to monitor the transfer of both electrons into the catalytic site. Systematic measurement of CcO reduction by hexaamineruthenium under anaerobic conditions revealed that the reduction of Cu_B accelerates ET to heme *a*₃ relative to the rate of entry of the first electron. Furthermore, the data suggest that the biphasic reduction of heme *a*₃, interpreted earlier as the effect of redox state of Cu_B [7], is due to the presence of different populations of purified CcO and also that ET to the catalytic site is dependent on the reduction level of both heme *a* and Cu_A.

Based on the assumption that ET to heme *a*₃ during reductive phase is limited by the rate of proton transfer, our studies also indicate that proton access to the catalytic site is regulated by two factors: (i) by a group with a pK_a of 6.5 controlling proton entrance into the K channel and (ii) by the rate of proton diffusion through this channel [8].

Acknowledgments

Supported by the National Institutes of Health (GM 55807), the Robert A. Welch Foundation (C-636) and VEGA (3198).

References

- [1] T. Tsukihara, H. Aoyama, E. Yamashita, T. Tomizaki, H. Yamaguchi, K. Shinzawa-Itoh, R. Nakashima, R. Yaono and S. Yoshikawa, *Science* 272 (1996), 1136-1144.
- [2] M. Brunori, A. Giuffrè and P. Sarti, *J. Inorg. Biochem.* 99 (2005), 324-336.
- [3] H. Michel, *Biochemistry* 38 (1999), 15129-15140.
- [4] S. Fergusson-Miller and G.T. Babcock, *Chem. Rev.* 96(1996), 2889-2907.
- [5] R. Mitchell and P.R. Rich, *Biochim. Biophys. Acta* 1186 (1994), 19-26.
- [6] D. Parul, G. Palmer and M. Fabian, *Biochemistry* 44 (2005), 4562-4571.
- [7] M. Verkhovsky, J.E. Morgan and M. Wikström, *Biochemistry* 34 (1995), 7483-7491.
- [8] M. Antalík, D. Jancura, G. Palmer and M. Fabian, *Biochemistry* 44 (2005), 14881-14889.

Photogeneration of Singlet Oxygen by Hypericin in Complexes with Low Density Lipoproteins: An Infrared Phosphorescence Study

P. GBUR¹, S. KAŠČAKOVÁ¹, D. JANCURA¹, R. DĚDIC², J. HÁLA² AND P. MIŠKOVSKÝ^{1,3}

¹ Department of Biophysics, P. J. Šafárik University, Jesenná 5, 041 54 Košice, Slovakia.

² Department of Chemical Physics and Optics, Charles University, Ke Karlovu 3, 121 16 Praha 2, Czech Republic

³ ILC, Ilkovičova 3, 812 19 Bratislava, Slovakia.

e-mail: gbenik@gmail.com

Photosensitized generation of singlet oxygen (¹O₂) by molecules of a photosensitizer (pts) is a crucial process in photodynamic therapy (PDT). Upon administration into blood stream, photosensitizers associate predominantly with serum proteins (low density lipoproteins (LDL), human serum albumin (HSA)). The interaction of hypericin (Hyp), natural photosensitizing agent occurring in the plants of the genus *Hypericum*, with HSA has been already intensively studied [1-4], however only few works about physicochemical properties of Hyp bound to LDL have been published [5,6].

Special apparatus for infrared phosphorescence measurements [7] were engaged to monitor Hyp phosphorescence (895 nm) and ¹O₂ formation (1278 nm) under illumination of Hyp in complex with LDL at different Hyp/LDL molar ratios. We have demonstrated, that amount of produced ¹O₂ increases linearly with Hyp concentration until ratio Hyp/LDL is about 20:1. Beyond this point the formation of ¹O₂ shows saturation behavior (saturation level reached cca. at molar ratio Hyp/LDL=75:1). With respect to this result we suggest, that the amount of produced ¹O₂ depends on the quantity of monomeric molecules of Hyp bound inside the lipidic part of LDL. The dependence of the intensity of Hyp phosphorescence on Hyp/LDL ratio is analogous with that for ¹O₂ formation.

We attempted to correlate these recent data with our previous results containing information about the concentration and light dose dependence of Hyp photosensitized oxidation of LDL [6]. Our effort is to build up coherent model describing ¹O₂ formation and biological activity of Hyp inside LDL particles.

Acknowledgement

This work was supported by the research grant from the Slovak Grant Agency Vega No. 2265. and APVT-20-036104.

References

- [1] P. Miskovsky, D. Jancura, S. Sanchez-Cortes, E. Kocisova and L. Chinsky, *J. Am. Chem Soc.* 120 (1998), 6374-6379.
- [2] K. Das, A. V. Smirnov, J. Wen, P. Miskovsky, J. Petrich, *Photochem. Photobiol.* 69 (1999), 633-645.
- [3] P. Miskovsky, J. Hritz, S. Sanchez-Cortes, G. Fabriciova, J. Ulicny and L. Chinsky, *Photochem. Photobiol* 74 (2001), 172-183.
- [4] B. Schwarzwinger, H. Falk, *Monatsh. Chem.* 134 (2003), 1353-1358.
- [5] G. Siboni, H. Weitman, D. Freeman, Y. Mazur, Z. Malik and B. Ehrenberg, *Photochem. Photobiol. Sci.* 1 (2002), 483-491.
- [6] S. Kascakova, M. Refregiers, D. Jancura, F. Sureau, J. C. Maurizot, P. Miskovsky, *Photochem. Photobiol.* 81 (2005), 1395-1403.
- [7] R. Dedic, A. Svoboda, J. Psencik, J. Hala, *J. Mol. Struct.* 301 (2003), 651-653 C.

Optical spectra of photoactive drug naphthazarin in solutions

M.SAVKO AND J. ULIČNÝ

Department of Biophysics, Faculty of Natural Sciences UPJŠ, Košice

Naphthazarin (NZ) (fig.1) is a photoactive drug naturally occurring in several exotic plants [1,2]. The interest for NZ is based on the fact, that structure of this molecule was found in numerous drugs with antitumoral and antiviral activity, such as daunomycin and adriamycin [3]. Moreover, NZ can induce apoptosis and it shows antimicrobial activity (as well as many larger derivatives of this molecule, making NZ an interesting model system).

Set of computations at various levels of theory (ZINDO[6], CIS[7], TD-DFT [8-13]) was performed to determine theoretically excitation energies for neutral (both C_{2v} and C_{2h} symmetry tautomers), monoanionic and dianionic forms of naphthazarin. Computations were performed for gas phase as well as in solutions (water and DMSO) modeled implicitly (Polarizable Continuum Model – PCM [14]) and explicitly involving several solvent molecules on configurations obtained from molecular dynamics simulations (based on analysis of spatial distribution functions). Results obtained via TD-DFT methodology were found to be of superior quality with respect to other approaches used in this study. Thus all conclusions presented below are relevant to that method.

Good overall match with experiment was attained with deviation less than 0.3 eV. Excitation energies computed for neutral form were found to be in very good agreement with experimental data for *in vacuo* computation and even better match was attained for implicit solvent computations. Excitation energies for anionic forms were shifted to the red with respect to the neutral form in accordance with experiment. Moreover, excitation for dianionic form was correctly computed to lie slightly below that of monoanionic form.

Inclusion of solvent effect via PCM method shifted excitation energies for neutral form very slightly to higher energies (differences $\sim 0.01\text{eV}$). Much more significant effect of inclusion of implicitly modeled solvent reveals results of computations for monoanionic and dianionic forms: $\sim +0.3\text{ eV}$ shift for monoanionic form and $\sim +0.1\text{ eV}$ for dianionic form.

Inclusion of solvent effects by computation with explicit solvent molecules had generally very strong effects on positions as well as on oscillator strengths of computed excitations. Excitations were generally shifted to near infrared what is inconsistent with experimental data. Strong disagreement with experiment suggests that method used to construct input configurations needs to be checked.

Acknowledgement

This work was supported by the VVGS grant of University of P.J. Safarik in Kosice No. 215/2005.

References

- [1] M. Moir, R.H. Thomson, *Phytochemistry* 12 (1973) 1351.
- [2] A. Ohta, P.M. Sivalingham, S. Lin, N. Ikekawa, N. Yaginuma, Y. Inada, *Toxicon* 11 (1973) 235-241.
- [3] Y.H. Mariam, R. Musin, *J. Mol. Structure: THEOCHEM* 586(1-2), 123, 2001.
- [4] P.M. Rentzepis, V.E. Bondybey, *J. Chem. Phys.* 80, 4727, 1984.
- [5] Kascakova, Gbur, Jurasekova, Department of biophysics, Institute of physics, University of P.J. Safarik in Kosice, unpublished.
- [6] E. Pereira, *Chem. Rev.* 8, 10, 1998.
- [7] M. C. Zerner, in *Rev. Comp. Chem.*, Ed. K. B. Lipkowitz and D. B. Boyd, Vol. 2 (VCH Publishing, New York, 1991) 313-366.
- [8] J. B. Foresman, M. Head-Gordon, J. A. Pople, and M. J. Frisch, *J. Phys. Chem.* 96, 135 (1992).
- [9] P. Hohenberg and W. Kohn, *Inhomogeneous Electron Gas*, *Phys. Rev.* 136, B 864, 1964.
- [10] W. Kohn and L.J. Sham, *Phys. Rev.* 140, A 1133, 1965.
- [11] A. Becke, *J. Chem. Phys.*, 98, 1372, 1993.
- [12] E. Runge and E.K.U. Gross, *Phys. Rev. Lett.* 52, 1984.

- [13] M. Petersilka, U.J. Grossmann and E.K.U. Gross, Phys. Rev. Lett. 76, 1996.
- [14] S. Miertuš, E. Scrocco, J. Tomasi, Chem. Phys., 55, 117, 1981.

Mitochondrial redox responses in isolated rat cardiomyocytes studied by spectrally and spatially resolved intrinsic flavin fluorescence.

J. KIRCHNEROVÁ¹, M. CAGALINEC², D. CHORVÁT.JR², A. CHORVÁTOVÁ³

¹Faculty of Mathematics, Physics and Informatics, Comenius University, Mlynská dolina, Bratislava, Slovakia.

²International Laser Centre, Ilkovičova 3, 812 19 Bratislava, Slovakia.

³Centre de Recherche, Hôpital Sainte-Justine, Montreal, Canada.

e-mail:kirchnerova@ilc.sk

Introduction. Main sources of cell autofluorescence, when excited by visible light, are resulting from oxidized mitochondrial flavins and flavoproteins. These molecules have overlapping emission spectra in the wavelength region of 490-560 nm [1,2]. Their redox fluorimetry is based on the loss of flavin fluorescence in reduced state.

Aim. We aim to develop tool for investigation of mitochondrial respiration in living cells based on spectrally and spatially resolved intrinsic fluorescence.

Materials and Methods. Cardiac myocytes were isolated following retrograde perfusion of the heart with proteolytic enzymes [3]. Spectral and spatial distribution of autofluorescence was recorded using laser scanning confocal microscope LSM 510 Meta (Zeiss) with C-Apochromat 40x/1,2 water immersion objective, in response to excitation by 458 nm Ar:ion laser line (Lasos Lasertechnik).

Results and Discussion. To demonstrate the sensitivity of cardiomyocyte autofluorescence to changes in the mitochondrial redox state, we applied 4 mmol/l sodium cyanide (NaCN), a blocker of respiratory chain at the level of complex IV, and 50 μ mol/l 2,4-dinitrophenol (DNP), mitochondrial uncoupler (Fig. 1). The decrease of flavin fluorescence after application of NaCN was caused by reduction of flavins due to blocked electron transport in the chain. The increase of flavin fluorescence after application of DNP was caused by oxidation of present flavins due to uncoupling of mitochondrial respiration. In regard to substantial photobleaching of autofluorescence due to consecutive scanning of single cell without observing spontaneous or induced recovery, in the next experiments we collected emission spectra from the first scans only.

To gather emission spectra related to mitochondrial metabolism and respiration we applied modulators and/or substrates specific for individual levels and pathways, which implicate flavin cofactors (Scheme 1). First, to discriminate between flavoproteins tightly bound to the respiratory chain below the complex I from the flavoproteins that are reduced via ubiquinone above the complex I, we applied sequence of 10 μ mol/l rotenone, blocker of respiratory chain at level of complex I and 4 mmol/l NaCN (Fig. 1).

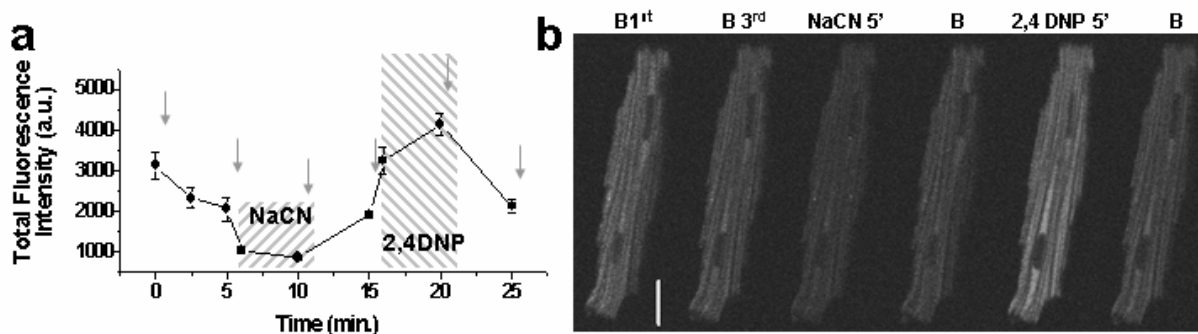
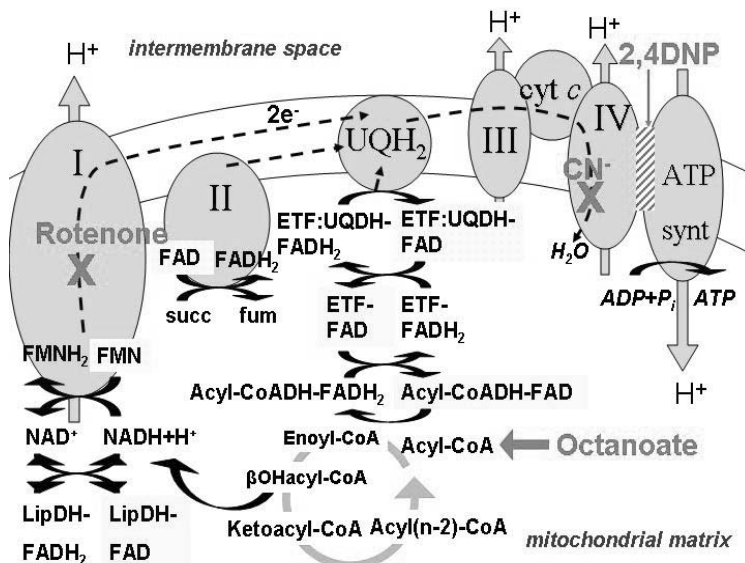


Figure 1 a Timecourse of total autofluorescence intensity (λ_{exc} 458nm / λ_{em} 477nm-638nm) response of cells (n=7) perfused with basic external solution and solution containing 4 mmol/l NaCN or 50 μ mol/l DNP at five

minute intervals indicated by the hatched fields. **b** Multispectral images of autofluorescence of the same cell obtained at different times of modulation as indicated by arrows in (a). White bar corresponds to 20 μm .



Scheme 1 Scheme of mitochondrial respiratory chain complexes and sites of action of applied mitochondrial modulators rotenone, sodium cyanide, octanoate and 2,4-dinitrophenol.

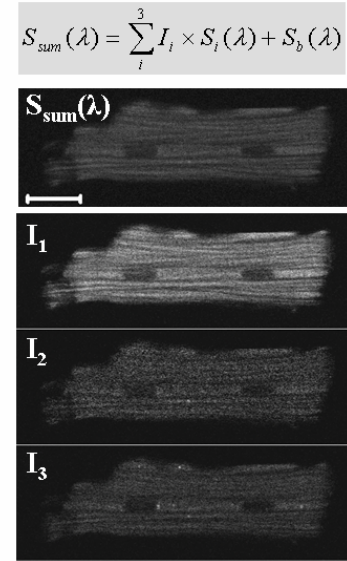


Figure 2 Application of linear unmixing algorithm on multispectral image of cell autofluorescence: spatial distribution of colour-coded intensity of individual weighting coefficients (I_i).

The decrease of autofluorescence after application of rotenone, observed in green region, is related to reduction of α -lipoamid dehydrogenase (LipDH) pool. Further decrease observed in the blue spectral region after application of NaCN was predominantly due to reduction of electron-transfer flavoprotein (ETF). The remaining spectral peak with maximum at 550nm was responsive to addition of 5mmol/l medium chain fatty acid octanoate in the rotenone pretreated cells. We hypothesize that acyl-CoA dehydrogenase (acyl-CoADH) could be responsible for the origin of this signal. Abrupt increase of autofluorescence mainly in the green spectral region with maximum at 530 nm caused by oxidation of free flavins and flavoproteins was induced by 50 $\mu\text{mol/l}$ DNP [2].

To identify major spectral components in autofluorescence images of isolated cardiomyocytes, principal component analysis (PCA) was applied on individual spectra of modulated cardiomyocytes. The result, three distinct components with their spectral profiles, were ascribed to LipDH and ETF flavoproteins, free FAD and acyl-CoADH based on their responsiveness to specific modulators [2]. The knowledge of spectral profiles of spectrally overlapping individual autofluorescence components ($S_i(\lambda)$) enables us to monitor their changes simultaneously, yet separately, by applying linear unmixing algorithm [4] on multispectral images of cell autofluorescence. The result of this approach is spatial distribution of colour-coded intensity of individual weighting coefficients (I_i) (Fig 2).

Conclusions. We have successfully applied multispectral imaging on the study of changes in autofluorescence in response to mitochondrial modulators. By application of PCA on obtained spectra and subsequent linear unmixing, we created a new tool for investigation of oxidation-reduction properties of isolated cardiomyocytes on subcellular level.

Acknowledgement

This work was supported by the research grant from the Slovak Grant Agency Vega No. 1/3406/06. AC is a FRSQ (N^o 2948) fellow supported by CIHR (MOP 74600).

References

- [1] D. Chorvat, Jr., V. Bassien-Capsa et al., *Laser Physics* 14 (2004), 220-230.
- [2] D. Chorvat, Jr., J. Kirchnerova et al., *Biophys J.* 89 (2005), L55-57.
- [3] A. Chorvatova and M. Hussain *Pflugers Arch.* 446 (2003) 422-428.
- [4] M. E. Dickinson, G. Bearman et al., *Biotechniques* 31 (2001), 1272-1278.

Study of resorcin[4]arene-dopamine complexation in mixed phospholipid monolayers

P. VITVIČ AND T. HIANIK

Department of Nuclear Physics and Biophysics, Faculty of Mathematics, Physics and Computer Sciences, Comenius University, Mlynská Dolina, 842 48 Bratislava, Slovakia
e-mail: palino1978@yahoo.com

We studied physical properties of monolayers formed by macrocyclic aromatic molecule resorcin[4]arene and its mixtures with dipalmitoyl phosphatidylcholine (DPPC) in various molar ratio formed at the air-water interface and at the presence of dopamine in water subphase by both surface pressure and dipole potential experimental techniques.

Due to the presence of the hydrophobic cavity, formed by the phenolic units, calixarenes are being used for detection of the various materials in the range from the ions to the biomacromolecules [1 – 3]. In the last years substantial attention is focused on the development of the methods for the detection of the neurotransmitters adrenaline, dopamine or ephedrine, Synthetic resorcin[4]arene has been found to be highly sensitive towards catecholamines with detection limit in μM concentration range [1, 4, 5].

Langmuir-Blodgett technique and dipole potential measurements showed, that resorcin[4]arene forms stable monolayers on the water subphase (Fig.1). The dipole potential reaches maximum (~ 125 mV) at the region corresponding to inflection point at π -A isotherm (at surface pressure of 5 mN/m). This suggests well-ordered monolayer already at relatively low surface pressure. At the maximum value of dipole potential, the surface dipole moment is approx. 0.5 D. Presence of dopamine resulted in an increase of mean molecular area and decrease of compressibility modulus of monolayers (Fig. 2.)

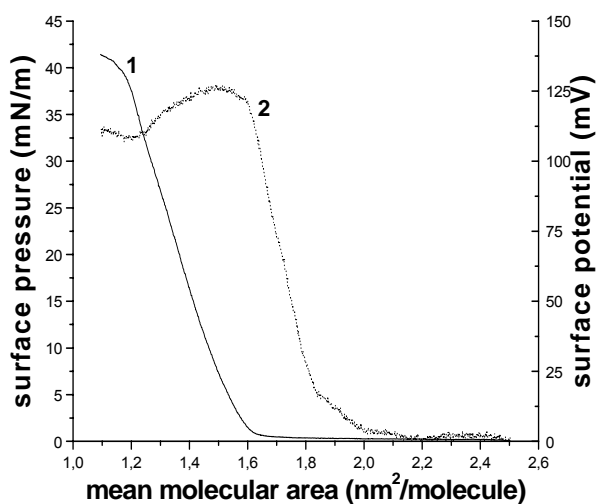


Fig.1 The plot of (1) surface pressure and (2) dipole potential as a function of mean molecular area for monolayers of pure resorcin[4]arene on the water subphase

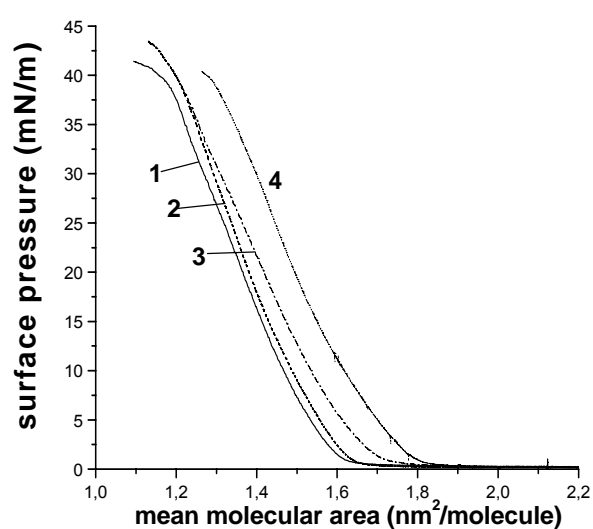


Fig. 2 The plot of surface pressure as a function of mean molecular area for monolayers of resorcin[4]arene at water subphase (1) and those contained dopamine in concentration: (2) - 10; (3) - 100 and (4) - 1000 μM , respectively

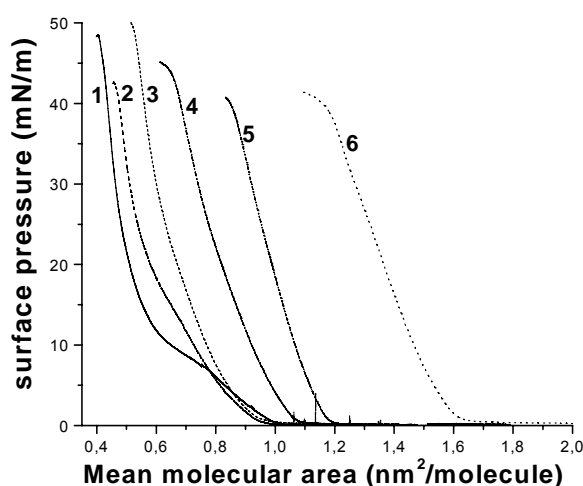
Thermodynamic stability of the monolayer formed on dopamine-containing subphase with the respect to the water subphase can be determined by the analysis of the excess of the Gibbs free energy [7]:

$$\Delta G = \int_0^{\pi} A_{dopa \min e} d\pi - \int_0^{\pi} A_{water} d\pi \quad (1)$$

ΔG values are positive and increase with increasing dopamine concentration, which indicates destabilization of the monolayers due to the complexation between the resorcin[4]arenes and dopamine even at the low concentration (10 μM). With increasing the dopamine concentration, the potentials shift towards higher dipole potentials due to the electrostatic interactions between dopamine and the resorcin[4]arene hydroxyl groups

DPPC/resorcin[4]arene form stable monolayers (Fig. 3). For mixed monolayers at higher content of resorcin[4]arene (>0.2 molar fraction) a positive deviations from ideal miscibility can be connected with formation of resorcin[4]arenes aggregates. Lowest miscibility and weakest interaction of dopamine with a monolayer was observed for 0.33 resorcin[4]arenes molar fraction in monolayer. (Fig. 4):

$$\Delta G^{ex} = \int_{\pi^0}^{\pi} A_{12} d\pi - X \int_{\pi^0}^{\pi} A_1 d\pi - (1-X) \int_{\pi^0}^{\pi} A_2 d\pi \quad (2)$$



(

Fig. 3 The plot of surface pressure as a function of mean molecular area for mixed DPPC/ resorcin[4]arene monolayers on the water subphase. 1:0 (1) (pure DPPC); 10:1 (2); 5:1 (3); 3:1 (4); 1:1 (4) and 0:1 (6) (pure resorcin[4]arene)

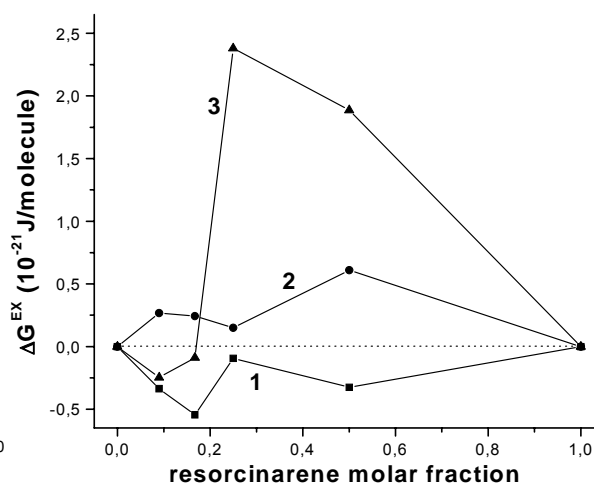


Fig. 4 Excess free energy, ΔG^{ex} , versus molar fraction of resorcin[4]arene in the DPPC monolayers calculated according to (2) at 1 – 5 mN/m, 2 – 15 mN/m and 3 – 35 mN/m

Acknowledgement

This work was supported by Science and Technology Assistance Agency under the contract No. APVT-51-013904, Ministry of Education of Slovak Republic under the project No. 9 conducted in framework of Slovak-Greece bilateral collaboration in Science and Technology.

References

- [1] D. P. Nikolelis, S.S.E. Petropoulou, E. Pergel, K. Toth, *Electroanalysis* 14 (2002), 783 – 789.
- [2] B. Lonetti, E. Fratini, A. Casnati, P. Baglioni, *Coll. Surfaces A* 248 (2004), 135 – 143.
- [3] D. Vollhardt, J. Gloede, G. Weidemann, R. Rudert, *Langmuir* 19 (2003), 4228 – 4234.
- [4] D.P. Nikolelis, D.A. Drivelos, M.G. Simantiraki, S. Koinis, *Anal. Chem.* 76 (2004), 2174 – 2180.
- [5] D.P. Nikolelis, C.G.Santorou, G. Theoharis, I. Bitter, *Electroanalysis* 17 (2005), 887 – 894.
- [6] G. Capuzzi, E. Fratini, F. Pini, P. Baglioni, A. Casnati, J. Teixeira, *Langmuir* 16 (2000), 188 – 194.
- [7] R. Maget-Dana, *BBA* 1462 (1999), 109 – 140.

Comparison of thermodynamic properties of release factors 2 from *Escherichia coli* and *Thermus thermophilus*

G. ŽOLDÁK¹, S. VÖRTLER², H. DOBBEK², N. GRILLENBECK², E. SEDLÁK¹ AND M. SPRINZL²

¹Department of Biochemistry, P. J. Šafárik University, Košice, Slovakia

²Laboratorium für Biochemie, Universität Bayreuth, Bayreuth, Germany

e-mail: sedlak_er@yahoo.com

Bacterial RF2 belongs to class I of RF that contains decoding factors. Functional mimicry between aminoacyl-tRNAs and class I RF implicitly suggested mimicry structural [1]. Both molecules need to recognize specific codons while simultaneously interact with the peptidyltransferase. This seemed to be analogous case of typical pair of structural and functional mimicry in translation: ternary complex of EF-Tu and translocational EF-G [2].

The first, and so far the only, structure of eubacterial RF2, from *E. coli*, provided unexpected surprises (Vestergaard et al. 2001). The GGQ peptidyl-tRNA hydrolysis and SPF anticodon motifs were only ~23 Å apart in the structure and not 75 Å, as expected. This finding not only mismatch with functional properties of RF2 but also shattered mimicry hypothesis regarding structural similarity RF2 and aminoacyl-tRNA (Ehrenberg and Tenson 2002, Kjeldgaard 2003). Release factor 2 (RF2) terminates protein synthesis by recognizing stop codons on mRNA *via* its conserved amino acid motif SPF and by conserved tripeptide GGQ interactions with the ribosomal peptidyltransferase center. As indicated by cryoelectron microscopy [3, 4], protein binds on ribosome in extended conformation and connects two sites remote 75 Å. The extended conformation is significantly different from the compact crystal structure of *E. coli* RF2 [5] (Fig. 1). Here, we present the crystal structure of homologous RF2 from *Thermus thermophilus*. The crystal structure of the thermophilic RF2 closely resembles structure of

RF2 from *E. coli* (Fig. 1). To provide more information about conformational properties of the RF2's, microcalorimetric, circular dichroism and fluorescence quenching studies have been performed on both proteins. A sequential biphasic thermal transition of mesophilic RF2 indicates domain structures. Proteins crystal structures and thermodynamic

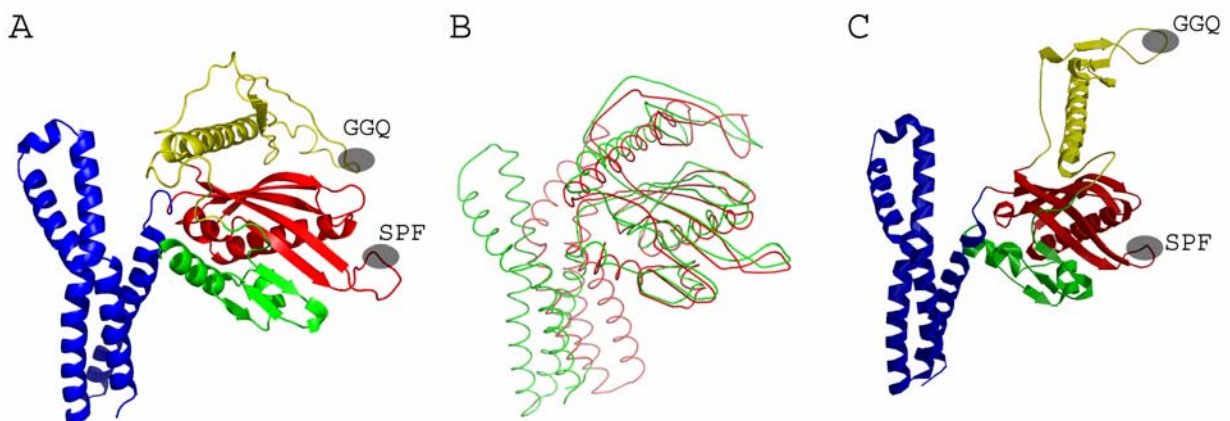


Fig.1 (A) Crystal structure of RF2 from *T. thermophilus*. (B) Comparison of crystal structures of RF2 from *T. thermophilus* and *E. coli*. (C) The extended conformation of RF2 from *E. coli* bound on ribosome.

analysis point to separated melting of domain I and domains II•III•IV. Thermophilic RF2 is characterized by: (i) stronger hydrophobic domain-domain interactions resulting in a single cooperative thermal transition; (ii) 30 °C higher transition temperature (Fig. 2); (iii) free energy difference higher by 48 ± 13 kJ/mol at 20 °C; and (iv) higher persistence against irreversible modification than its mesophilic ortholog. Notably, transition temperatures of both proteins are only few degrees above the corresponding physiological conditions and point to their conformational lability. Differences in stability, structure dynamics, sequence, purification strategy, crystallogenes and crystal packing between the *E. coli* and *T.*

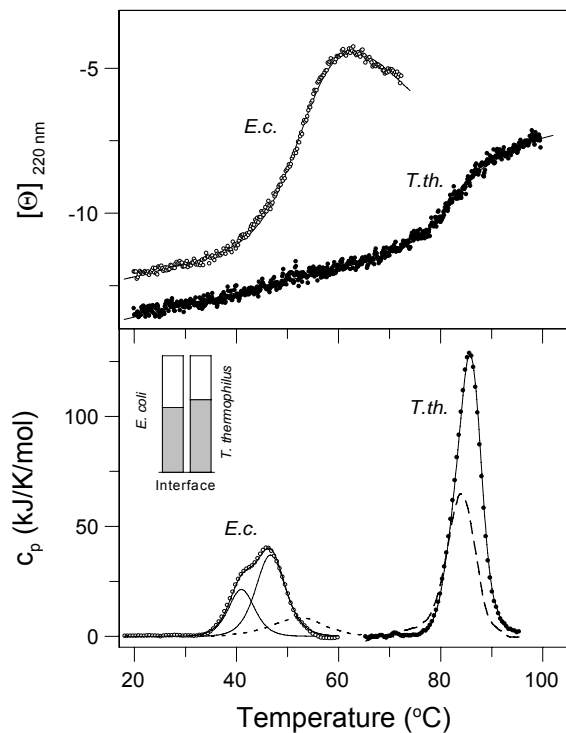


Fig. 2 Temperature induced denaturation of release factors monitored by circular dichroism and calorimetry. *Upper panel:* Protein ellipticity in the far-UV region of CD at 220 nm was used to monitor unfolding of secondary structure of release factors (*E.c.* and *T.th.*). Ellipticity $[\Theta]$ is shown in 10^{-3} deg.cm²/dmol units. *Lower panel:* Calorimetric scans of release factors (thick lines, *E.c.* and *T.th.*) were obtained upon subtraction of baselines. Second heating scans are shown as dashed line (*T.th.*) and dotted line (*E.c.*). Scan rate was 90 K/min. Both protein concentrations were 24 μM. Curve fits of thermal denaturation based on the single and multiple two state process are shown as solid line. *Inset:* Relative composition of Δ ASA of interfaces between domain I and domains II•III•IV of RF2's from *E.coli* and *T. thermophilus* – polar aminoacids (white box), nonpolar aminoacids (grey box).

thermophilus proteins strongly indicate that the compact conformation resemble a stable, relevant state in the absence of ribosome.

Acknowledgement

The authors would like to thank the Slovak Grant Agency for financial support through grant no. 1/0432/03 and Deutscher Akademischer Austauschdienst (DAAD) Nr. 00512972 and Fonds der Chemischen Industrie. We thank Norbert Grillenbeck for his technical assistance. We thank Mans Ehrenberg for the clone of RF2.

References

- [1] K. Ito, K. Ebihara, M. Uno and Y. Nakamura, *Proc. Natl. Acad. Sci. U.S.A.* 93 (1996), 5443-5448.
- [2] J. Nyborg, P. Nissen, M. Kjeldgaard, S. Thirup, G. Polekhina and B. F. C. Clark, *Trends Biochem. Sci.* 21 (1996), 81-82.
- [3] U. B. S. Rawat, A. V. Zavialov, J. Sengupta, M. Valle, R. A. Grassucci, J. Linde, B. Vestergaard, M. Ehrenberg and J. Frank, *Nature* 421 (2003), 87-90.
- [4] B.P. Klaholz, T. Pape, A. V. Zavialov, A. G. Myasnikov, E. V. Orlova, B. Vestergaard, M. Ehrenberg and M. van Heel, *Nature* 421 (2003), 90-94.
- [5] B. Vestergaard, L. B. Van, G. R. Andersen, J. Nyborg, R. H. Buckingham and M. Kjeldgaard *Mol. Cell* 8 (2001), 1375-1382.

Amino acid propensities for flavin adenine dinucleotide binding sites in proteins.

G. ŽOLDÁK¹, K. TÓTH¹ AND E. SEDLÁK¹

¹Department of Biochemistry, P. J. Šafárik University, Moyzesova 11, 041 54 Košice, Slovakia.
e-mail: kamil_toth@yahoo.com

A flavin adenine dinucleotide (FAD) is the most common member of a variety of derivatives of flavins in the cell. FAD is a major form of the flavin derivatives (riboflavin, FMN, etc.) [1]. Chromatographic determination of flavin content in the yeast estimate 71.5% of FAD [1]. Remarkably, about 65 % of flavoproteins (FMN, riboflavin, FAD) in Protein Databank are FAD contained proteins. Despite rapid progress in the knowledge of the functional importance of flavoproteins, our understanding of FAD binding to the protein, as regards both the properties of the FAD binding site in the protein and the properties of the bound FAD, is far from being complete. Several conserved sequence motifs and the occurrence of tyrosine and tryptophan residues close to flavin binding sites have also been found and characterized in flavoproteins [2, 3]. Sequence and structure analysis of a dataset of 32 nonhomologous FAD containing proteins showed four different families of FAD-structural patterns [3]. There is no general conserved sequence for FAD binding and recognition; however several conserved sequence motifs were found within structural families: glutathione reductase - GR, ferredoxin reductase - FR, p-cresol methylhydroxylase – PCMH, pyruvate oxidase and single member FAD folds – SM.

The variety of structures, functions and substrates bound to the binding sites of flavoproteins indicates that there might not be a “specific” sequence that binds the FAD cofactor. This is in agreement with the concept of a fuzzy recognition template suggested in an effort to describe the protein/adenylate interaction [4]. This concept proved to be useful and was confirmed in several reports where ligand recognition by proteins was studied [5, 6].

A nonhomologous dataset of flavin adenine dinucleotide (FAD) containing proteins was chosen to obtain a molecular picture of the protein/cofactor interactions, conformation of the cofactor in the binding site of the flavoproteins, and amino acid propensities for FAD binding sites in proteins [7]. Generally, three different types of amino acids propensities may be distinguished: (1) negative propensity, $P_i < 0$, i.e. relative occurrence of the given amino acid is lower than expected from relative composition of the whole sequence; (2) neutral propensity, $P_i=0$, which indicate that relative occurrence of the given amino acid inside the FAD binding site is the same as in sequence; and (3) positive propensity, $P_i > 0$, i.e. amino acid occurs at higher frequency inside FAD binding site than expected from relative composition of the sequence. Thus, the propensity reflects the enrichment of the amino acid inside FAD binding sites against the background - relative composition of the whole sequence. Glycin, arginine, asparagine, serine, cysteine, threonine, histidine, tyrosine, and tryptophan show a positive propensity for interactions with FAD. The amino acid propensities for isoalloxazine ring, ribityl chain, ADP and whole FAD were also calculated. In summary; (1) glycine, arginine, threonine, tyrosine and tryptophan have positive propensity for all parts of FAD; (2) alanine, valine, leucine, isoleucine, glutamate, glutamine have negative propensity for all part of FAD; and (3) the rest of amino acids have display mixed propensities for individual parts of FAD, e.g. proline has negative propensity for ADP and isoalloxazine part, but positive propensity for ribityl chain. The overall propensities for FAD reflect propensities of the all three parts and they are likely weighted according their energetic contribution. High occurrence of the glycine was found to be due to the inherent flexibility of the backbone chain that allows it to be in the specific region of the Ramachandran graph

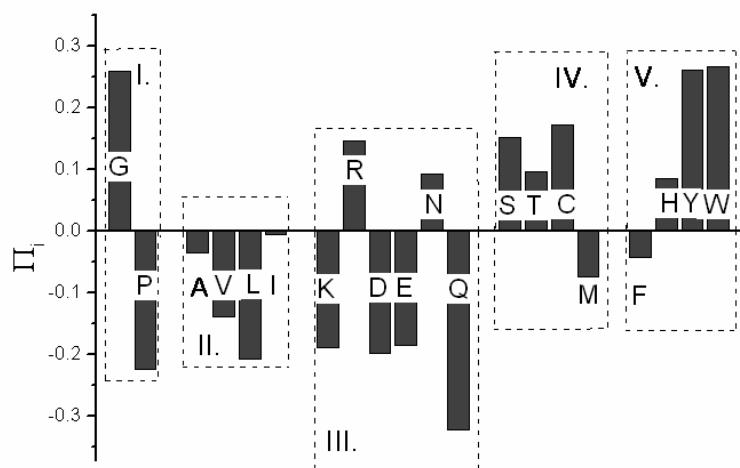


Fig. 1 Amino acids propensities for the whole FAD. Amino acids were divided into five groups: (I) glycine and proline; (II) alanine, valine, leucine and isoleucine; (III) lysine, arginine, aspartate, glutamate, asparagines and glutamine; (IV) serine, threonine, cysteine and methionine; (V) phenylalanine, histidine, tyrosine and tryptophan.

where other amino acid residues cannot be. The presence of the aromatic residues inside FAD binding sites indicates a common structural/functional role of stacking interactions in flavoproteins. The pattern of the distance distribution of the hydrogen bonds shows two maxima, one at 2.8 Å and the other at 4.3 Å. Only 46-71% of donors and acceptors of FAD can satisfy the hydrogen bonding potential at the distance of 2.8 Å, and the rest form weaker interactions. The tendency of the FAD cofactor to minimize solvent accessibility is evident from the observation that ~98% of the accessible surface area of FAD is usually

buried within the monomeric subunit. Flavin molecules are found in a variety of conformations. The cofactors were roughly classified according to their radius of gyration into two forms: bent and elongated. Up to 80 % of FAD is in the bent form in aqueous solution and only 25% is bent inside of the flavoproteins. Increasing the radius of gyration of the FAD cofactor is accompanied by an increase in the protein/cofactor contact area, and a slight improvement in the hydrogen bonding potential of FAD.

Acknowledgement

The authors would like to thank the Slovak Grant Agency for financial support through grant no. 1/0432/03.

References

- [1] A. Gliszczynska and A. Koziolowa, *J. Chromatogr. A* 822 (1998), 59-66.
- [2] M. Inoue, M. Shibata, Y. Kondo and T. Ishida, *Biochemistry* 20 (1981), 2936-2945.
- [3] O. Dym and D. Eisenberg, *Protein Sci.* 10 (2001), 1712-1728.
- [4] S.L. Moodie, J.B. Mitchell and J.M. Thornton, *J. Mol. Biol.* 263 (1996), 486-500.
- [5] I. Nobeli, R.A. Laskowski, W.S. Valdar and J.M. Thornton, *Nucleic Acids Res.* 29 (2001), 4294-4309.
- [6] V. Čappello, A. Tramontano and U. Koch, *Proteins* 47 (2002), 106-115.
- [7] G. Žoldák, K. Tóth and E. Sedlák, *Biochem. Biophys. Acta* submitted.

Dynamics of active site of NADH oxidase from *Thermus thermophilus*: experiments and molecular dynamics

J. HRITZ^{1,2}, G. ŽOLDÁK¹ AND E. SEDLÁK¹

¹ Department of Biochemistry, P. J. Šafárik University, Moyzesova 11, 04001 Košice, Slovakia.

² Leiden/Amsterdam Center for Drug Research, Division of Molecular Toxicology, Vrije Universiteit Amsterdam, Netherlands.

e-mail: sedlak_er@yahoo.com

NADH oxidase (EC 1.6.99.3) (NOX) from *Thermus thermophilus* is a member of the novel structurally homologous flavoprotein family of flavin reductases and nitroreductases [1]. This family of nitroreductases attracts intense attention in medicine, industry and environmental chemistry [2,3]. Nitroreductases and homologous enzymes reduce substrates through a bi-bi ping-pong kinetic mechanism as observed in nitroreductases that reduced nitroaromatic to nitrosoaromatic compounds [2]. The ability to modulate (inhibit or activate) the activity of the flavin reductases and nitroreductase is of interest to medicinal and biotechnological researchers. NOX from *T. thermophilus* is stable in extremes of heat, pH and chaotropic agent concentration [4-7]. The enzyme catalysis includes hydride transfer from NADH to the intrinsic flavin cofactor. The intrinsic flavin cofactor is recycled by extrinsic co-substrates such as FMN and FAD. Dynamics of the active site was studied (1) **by experimental techniques** [4-7]; and (2) **by the molecular dynamics simulation** [8].

(1) Recent investigations demonstrated that the presence of a chaotropic reagent such as urea, Hofmeister series of anions and pH changes produce an enhancement of the activity of NOX at room temperature [4-7]. We have shown that perturbation of the enzyme active site by 1 M urea or a change in the pH of the protein solution from pH 7.0 to 5.0 led to a ~2.5 and ~2.0 fold increase in the enzyme activity, respectively. Results obtained from the circular dichroism showed that the global conformation of the protein was unaffected by the 1 M urea. Fluorescence of tryptophanes shows fine perturbation of the tertiary structure. Modulation of the activity of NOX can be even more sensitively tuned by the Hofmeister series of anions. The data demonstrate that the high rigidity of the active site in the presence of kosmotropic anions, and its great flexibility in the presence of chaotropic anions each have a decelerating effect on the enzyme activity. Based on the experimental data and the structure analysis we suggested that the local movement of the indol ring of Trp47, located in the active site of the enzyme, is the reason for the increase in enzyme activity in the presence of urea.

(2) Three different sets of molecular dynamics (MD) simulations were performed: 1. NOX in water solution starting from the crystallographic conformation, 2. NOX in urea solution starting from the crystallographic conformation, 3. NOX in urea solution starting from the state in which catalytic site is in the closed conformation. Each of these MD simulations sets contains 10 independent MD runs (different initial atom velocities) of the length of 12 ns, in 2 of them electrostatic interactions were treated by Particle Mesh Ewald (PME) and 3 of them were prolonged up to 18 ns time length. As a global structural parameters Rg, and RMSD of the protein backbone were calculated. Their time evolutions show that structures of NOX in water and 1M urea solution were stable and similar during whole time of MD simulations. In both simulations Rg of NOX was nearly constant over the time, $\langle Rg \rangle = 1.99$ nm. In addition, secondary structure of each residue over the time of simulations was calculated, which shows that their secondary structure remained stable during whole time of MD simulations. The open and closed conformations could be differentiated by the distance between the planes of Trp47 and FMN412 (Fig. 5A). The process of closing the active site was very fast, about 60 ps, and correlated with release of the bound water molecule from the active site. In the open conformation, the water molecule is strongly bound between Trp47 and FMN412 by two hydrogen bonds between the backbone NH group of Trp47 and

the water oxygen and between the water and the hydroxyl group of FMN412. In 10

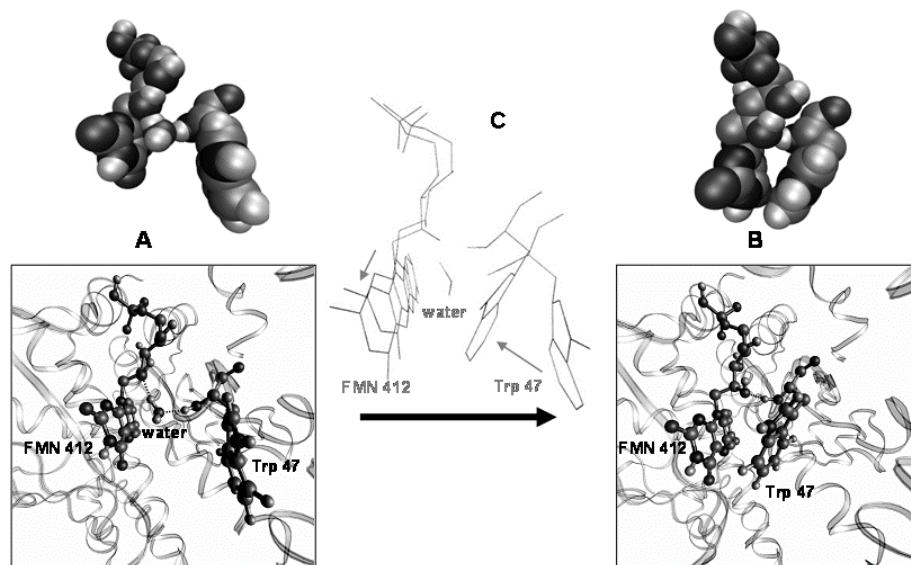


Fig. 1 Molecular model of the catalytic site of NOX in water. (A) open and (B) closed conformation of the catalytic site between Trp47 and FMN412. For clarity Trp47, FMN 412 and the water molecule bound between them are shown in detail. The rest of protein is in the ribbons form. Dashed lines are hydrogen bonds critical for the interaction between Trp47 and FMN412. Above corresponding figure, Trp47 and FMN 412 are also shown in van der Waals representation. (C) Both conformations of the active site after alignment of the protein backbones. Structural changes occurring during the closing event are indicated by dark grey arrows.

independent simulations of NOX in water solution we have observed closing of the active site in 9 of them for the first catalytic site and in 7 of them for the second catalytic site in the symmetrical unit. Analysis of the MD trajectories of NOX in 1M urea revealed the molecular mechanism that prevented closure of the catalytic site. In all MD simulations of NOX in 1M urea, we have observed the fast binding of a urea molecule between Trp47 and FMN412, occurring in two steps. In the first step the urea molecule formed a stable hydrogen bond coming from the carbonyl group to the water molecule bound between FMN and Trp47 in the active site. After the formation of this complex the orientation of the water molecule changed and was not favorable to form both the hydrogen bonds to Trp47 and FMN412, as in the absence of urea. The presented molecular modeling data [8] are in good agreement with our previous experimental results [4-7] and confirm the proposal that: (i) Trp47 is important for enzyme catalysis and substrate binding; and (ii) urea opens the active site without perturbing the overall structure of the protein.

Acknowledgement

The authors would like to thank the Slovak Grant Agency for financial support through grant no. 1/0432/03 and 1/3252/06, HPC-Europe (RII3-CT-2003-506079), with the support of the European Community-Research Infrastructure Action under the FP6 "Structuring the European Research Area" Program for sponsoring research stay of J.H. in SARA supercomputer center in Amsterdam and Linda Sowdal for her invaluable editorial help in preparing the manuscript.

References

- [1] A.G. Murzin, S.E. Brenner, T. Hubbard, C. Chothia, *J. Mol. Biol.* 247 (1995), 536-540.
- [2] G.N. Parkinson, J.V. Skelly, S. Neidle, *J. Med. Chem.* 43 (2000), 3624-3631.
- [3] E.P. Best, G.K. Kvesitadze, G. Khatishvili, T. Sadunishvili, *Z. Naturforsch.* 60 (2005), 340-348.
- [4] G. Žoldák, R. Sut'ak R, M. Antalík, M. Sprinzl, E. Sedlák, *Eur. J. Biochem.* 2003; 270: 4887-4897.
- [5] G. Žoldák, M. Sprinzl, E. Sedlák, *Eur. J. Biochem.* 271 (2004), 48-57.
- [6] G. Žoldák, A. Musatov A, Stupák M, Sprinzl M, E. Sedlák, *Gen Physiol Biophys* 24 (2005); 279-298.
- [7] M. Stupak, G. Žoldák, A. Musatov, M. Sprinzl, E. Sedlák, *Biochim Biophys Acta.* 2006 Jan;1764(1):129-37.
- [8] J. Hritz, G. Žoldák, E. Sedlák, *Proteins: Structure, Functions and Bioinformatics* (2006) (in press).

Imaging of polymer distribution in polyelectrolyte microcapsules using covalently bound fluorescent markers and confocal laser scanning microscopy

J. PODSKOČOVÁ¹, D. CHORVÁT, JR.², G. KOLLÁRIKOVÁ³ AND I. LACÍK³

¹ Faculty of Mathematics, Physics and Informatics, Comenius University, Bratislava, Slovakia.

² ILC, Ilkovičova 3, 812 19 Bratislava, Slovakia.

³ Polymer Institute of the Slovak Academy of Sciences, Bratislava, Slovakia.
e-mail: podskocova@ilc.sk

Introduction: Permanent deficit of human tissue and organ donors led to formation of new application of polymers in medicine – immunoisolation. The most perspective immunoisolation technology today is encapsulation in microcapsules [1]. It means an enclosing of biological material into the polyelectrolyte capsule, at preservation of its viability and catalytic activity, with the aim to implant this immobilized material without using of immunosuppressives, and treat the diseases caused by failure of secretion activity of own cells. An encapsulation material acts as a semipermeable membrane for a controlled transport of species to and from the encapsulated biological material in a desired way. Surface quality and microstructure of capsules determine their appropriateness for successful medical applications. Therefore, it is important to reliably characterize the individual types of capsules considering their inner structure and surface.

Aim: Imaging of polymer distribution in polyelectrolyte microcapsules using confocal laser scanning microscopy.

Material and methods: Formation of studied microcapsules is based on reaction of opposite charged polymers containing covalently bound anionic (sodium alginate and cellulose sulfate) and cationic (poly(methylene-co-guanidine)) groups. Microcapsules [2] were produced by dropping the polyanion solution, made of sodium alginate (SA) and cellulose sulfate (CS), to the solution of poly(methylene-co-guanidine) (PMCG), CaCl₂ and NaCl at pH 7.0. Capsules were fluorescently labeled following labeling protocols described by Lamprecht et al. [3] and Strand et al. [4] and visualized using confocal laser scanning microscopy. The reflection and fluorescence emission were measured by confocal laser scanning microscope LSM510 META on Axiovert 200 (Zeiss) using 40x/1.2W C-Apochromat objective.

Results and discussion: In our previous research [5] we studied spatial distribution of polymers in capsules using anionic (Eosin Y) and cationic (Rhodamine 123) labels specifically bound by electrostatic interactions to the residual charge of the polymers in the capsule. This experiment resulted in identification of a profile of the respective label, which may reflect the distribution of a polymer with opposite charge. To verify this assumption, the capsules with covalently labeled polymers were prepared. Figure 1 shows fluorescence emissions from capsules prepared from covalently labeled PMCG, SA and CS. Figure 2 shows intensity profiles of fluorescence of covalently labeled PMCG, CS, SA and specifically bound labels of the opposite charge to polycation (PMCG) and polyanions (SA and CS). This figure demonstrates that while the profiles of covalently and non-covalently labeled polycation is similar, there exist some noticeable differences in the intensity profiles of covalently and specifically labeled polyanion.

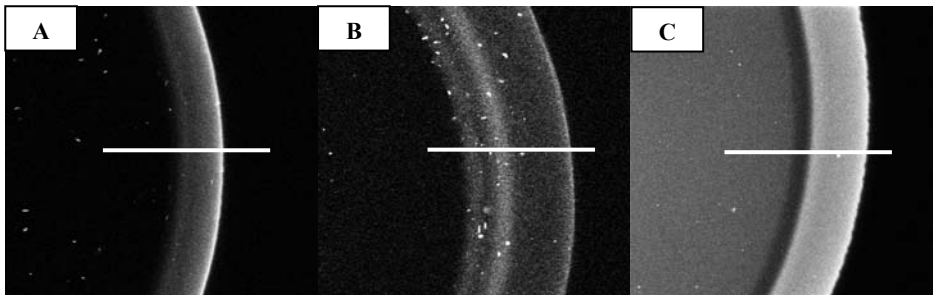


Fig. 1 Microcapsules with covalently labeled PMCG (A), CS (B) and AS (C) in the.

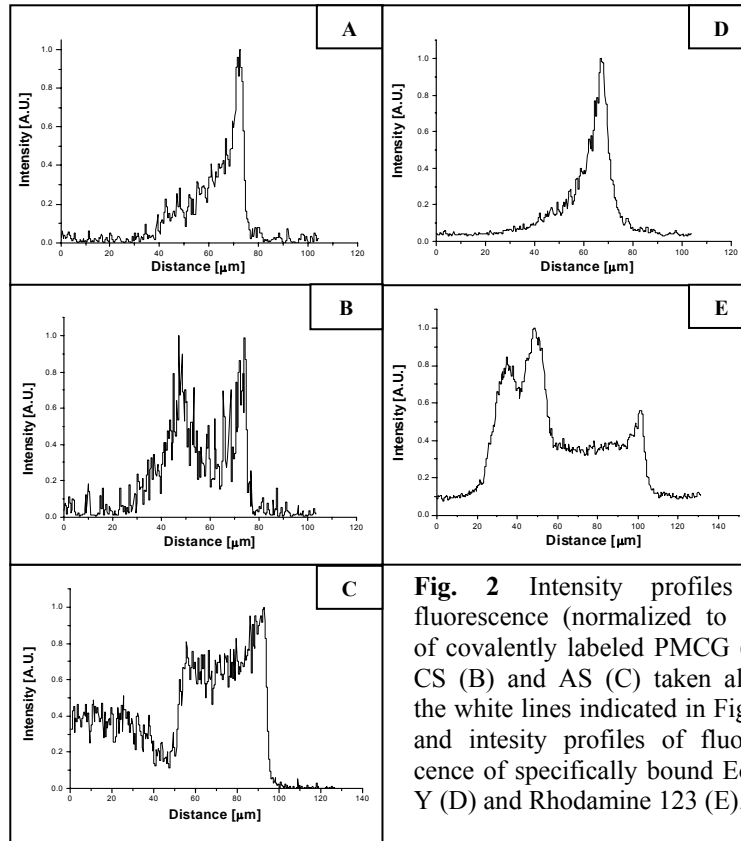


Fig. 2 Intensity profiles of fluorescence (normalized to 1.0) of covalently labeled PMCG (A), CS (B) and AS (C) taken along the white lines indicated in Fig. 1, and intensity profiles of fluorescence of specifically bound Eosin Y (D) and Rhodamine 123 (E).

Conclusions: In this contribution we demonstrated that confocal laser scanning microscopy with covalently bound fluorescent labels is a very useful tool for imaging of polymer distribution in microcapsules. Specifically bound labels show pattern probably corresponding to the distribution of free charged groups in unfixed polymer chains.

Acknowledgement

This work was supported by Science and Technology Assistance Agency under the contract No. APVT-20-016002.

References

- [1] Q. Hou, Adv. Drug. Delivery Rev. 1999. 35: p. 271.
- [2] I. Lacik et al., J. Biomed Mater Res, 1998. 39(1): p. 52.
- [3] Lamprecht et al., Eur. J. Pharma, Biopharma 2001. 49: p. 1.
- [4] Strand et al., Biotechnol. Bioeng. 2003. 82: p. 386.
- [5] J. Podskocova et al., Laser Physics 2005. 15(4): p. 545.

Estimation of single cardiomyocyte volume by active contour algorithm

M. CAGALINEC¹, A. MATEAŠIK¹, A. CHORVÁTOVÁ^{2,3} AND D. CHORVÁT JR.¹

¹ International Laser Centre, Ilkovičova 3, 812 19 Bratislava, Slovakia.

² Research Centre of Sainte-Justine Hospital, Montreal, Canada.

³ Department of Pediatrics, University of Montreal, Montreal, Canada
e-mail: misoc@ilc.sk

Introduction: Precise determination of cardiomyocyte volume is essential for comprehension of many aspects of cardiac physiology and pathophysiology. Despite this fact, simple and unified techniques that allow estimation of the single cardiomyocyte volume with sufficient precision are still limited. To overcome currently used empirical approach based on simple geometric approximation or interactive detection of the myocyte border, we examined possible use of automated segmentations techniques [1] for single cardiomyocyte volume estimation. Our aim was therefore to apply an analytical approach to assess volume of isolated cardiomyocytes from 3D confocal images.

Materials and methods: The work was done on Wistar rats (Dobra Voda). Left ventricular cardiomyocytes were isolated following retrograde perfusion of the heart with proteolytic enzymes [2]. Confocal images of isolated myocytes were obtained by laser scanning confocal microscope LSM 510 Meta (Zeiss) after staining with Fluo-3 fluorescent probe (1 $\mu\text{mol/l}$, ex/em 488/515 nm). All computations were performed using the IBM Linux parallel cluster with computation libraries and scientific computing software (NAG).

Results and Discussion: For segmentation and determination of cell contour in single 2D slice, we have used an active contour model proposed by Kass et al. [3] (Fig. 1). When contours in all slices were known, all voxels belonging to space allocated by contours were summed and the sum was taken as the cell volume. Rendered shape of the cardiomyocyte calculated from 3D confocal data (Fig. 2B) is demonstrated at Fig. 2C.

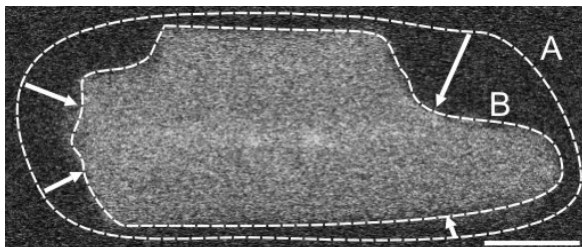


Fig. 1 Cardiomyocyte shape segmentation in single 2D slice by active contour algorithm. Initial shape is identical with image borders. A) 2nd iteration, B) final iteration. Bar: 20 μm .

To estimate the dependence of the contour algorithm on settings of the confocal microscope, we have tested fluorescent labeled spheres (Focal-Check Microspheres, Molecular Probes, 15 μm , ex/em 488/515 nm). As presented at Fig. 3A, pinhole diameter of 2 AU fitted the theoretical volume of the sphere. Detector amplifier gain did not influence the calculated volume (Fig. 3B). Laser illumination had only marginal effect on the sphere volume at intensities below 2

μW (1% of laser intensity, Fig. 3C). After application of the procedure to confocal image of the myocyte, we detected invaginations of the calculated shape to the inside of the myocyte, caused by low signal/background intensity ratio. To avoid underestimation of the cell volume, we have therefore applied Gaussian blurring (kernel radius 3) to confocal image before the segmentation procedure (Fig. 2C). In this way, we also tested the impact of blurring on the rendered volume of the sphere. Without blurring, the volume of the sphere was underestimated. With Gaussian blurring for kernel radius 3, the sphere volume was nearly identical with its theoretical value (Fig. 3D). To insure that the blurring did not lead to overestimation of the myocyte volume, we applied segmentation algorithm to myocytes stained with a different indicator: membrane probe di-8-ANEPPS (5 $\mu\text{mol/l}$, ex/em 488/>560

nm). No significant change in cell volumes was observed when Fluo-3 and di-8-ANEPPS stained myocytes were compared.

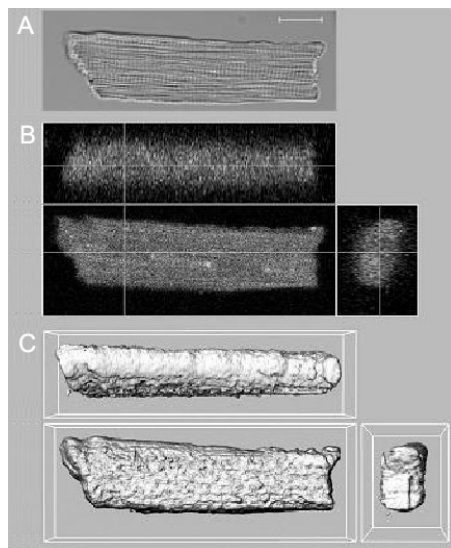


Fig. 2 Brightfield image (A), orthoslice of 3D confocal image (B) and rendered shape (C) of the isolated cardiac myocyte. Bar: 20 μ m.

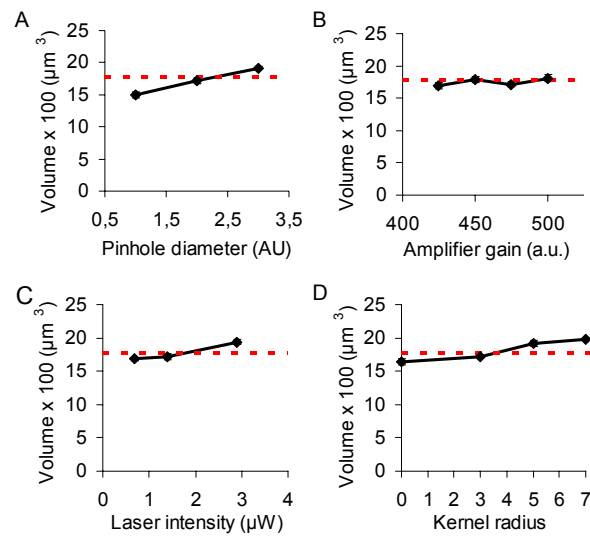


Fig. 3 Impact of confocal pinhole diameter (A), amplifier gain (B), laser intensity (C) and Gaussian blurring (D) on rendered volume of fluorescent sphere. Dashed line: theoretical volume of the sphere. Data are presented as mean \pm SD (N=3 spheres), SD is smaller than the symbols.

Conclusions: We demonstrated implementation of active contour algorithm, a method of automatic object segmentation, for estimation of volume of single cardiac myocytes stained with fluorescent indicator Fluo-3. By testing the procedure on model objects with known shape and volume, we optimized settings of the confocal microscope and the data processing (e.g. pinhole diameter and blurring). Described method was also successfully applied for myocyte volume calculation after staining with membrane indicator di-8-ANEPPS. Our results make this procedure a useful tool for myocyte volume estimation using another groups of fluorescence indicators.

Acknowledgement

This work was supported by the research grant from the Slovak Grant Agency Vega No. 1/3406/06.

References

- [1] L. Kubinova, J. Janacek, F. Guilak and Z. Opatrny, *Cytometry* 36 (1999), 85-95.
- [2] D. Chorvat Jr., V. Bassien-Capsa, M. Cagalinec, J. Kirchnerova, A. Mateasik, B. Comte and A. Chorvatova, *Las Phys* 14(2) (2004), 220-230.
- [3] M. Kass, A. Witkin and D. Terzopoulos, *Int. J. Comp. Vision* 1 (1988), 321-331.

Photodynamic therapy of gastrointestinal superficial polyps with aminolevulinic acid. A clinical and spectroscopic study

J. SMOLKA¹, A. MATEÁŠIK¹ AND P. MLKVY²

¹ International Laser Centre, Ilkovičova 3, 812 19 Bratislava, Slovakia.

² Department of Laser Medicine, St. Elisabeth Cancer Hospital, Heydukova 10, 812 50 Bratislava, Slovakia
e-mail: smolka@ilc.sk

Introduction: Photodynamic therapy (PDT) is a minimally invasive therapeutic modality approved for the treatment of neoplastic and vascular diseases [1]. It involves light-induced activation of administered photosensitizer in tissue to produce local necrosis or apoptosis [2]. Aminolevulinic acid (ALA) is an efficient substance used in photodynamic therapy. It is a precursor of light-sensitive product protoporphyrin IX (PpIX), which selective accumulation in malignant cells is due to the altered activity of the heme biosynthetic pathway enzymes in such cells [3]. Upon irradiation of PpIX energy of absorbed photons is partially transferred to molecular oxygen through a metastable triplet state and partially spent on fluorescence. Fluorescence is a useful tool for detection of accumulation of a photosensitizer in treated tissue what can be utilized in fluorescence diagnostics. The field of application of fluorescence diagnostics has been expanded after development of laser techniques. With fiber laser system it is possible to deliver and subsequently collect radiation from the places like oesophagus, stomach, intestine etc. An important part of clinical study and fluorescence diagnostics is fluorescence investigation of biopsies. However, the detected fluorescence image of cryoslit from biological sample with accumulated photosensitizer is a mixture of signals due to autofluorescence (originating from NADH, flavins, flavoproteins etc) and a signal from a photosensitizer [4]. These signals are possible to distinguish by using methods of spectrally resolved fluorescence microscopy and linear unmixing. This enables monitoring of the level of accumulation of photosensitizer in suspected area of tissue giving valuable information for improvement of the whole PDT procedure.

In the present study, we have applied ALA-based PDT for the treatment of superficial precancerous lesions in the area of oesophagus, stomach and intestine. In vivo fluorescence detection of photosensitizer accumulation in the tissue was performed by means of a novel fiber spectrometer. The results of in vivo fluorescence diagnostics were compared with fluorescence analysis of biopsies.

Subjects and Methods: Eight patients with superficial gastrointestinal adenocarcinoma lesions were involved in the present study. Patients were given 40 mg/kg ALA dissolved in 10 ml of fruit juice to drink. Four hours later in vivo measurements of accumulated PpIX in tissue was performed by fibre spectrometer LESA-01-BIOSPEC (JSC BioSpec) with He:Ne laser operating at 632.8 nm with power 2 mW. Biopsies were taken from which cryoslits were prepared. These were scanned by laser scanning confocal microscope LSM 510 Meta (Zeiss) with C-Apochromat 40x/1.2 water immersion objective. Spectroscopic measurements of sample fluorescence were performed in response to 458 nm Ar:ion and 633 He:Ne laser lines (Lasos, Lasertechnik), respectively. Linear unmixing methods were used to determine the regions of PpIX accumulation.

1. *In vivo fluorescence measurements:* In vivo fluorescence measurements performed 4 hours after ALA administration before PDT revealed increased fluorescence intensity in the suspected area of the tissue as compared to the adjacent normal mucosa (Figure 1A).

2. *Fluorescence microscopy:* Examples of spectral images of cryoslits from biopsies of superficial intestinal polyps are shown in Figure 1B. Areas of increased red fluorescence were clearly visible within suspected area. Corresponding fluorescence spectra were characterized

by maxima at around 633 nm and 675 nm after the excitation with 458 and 633 nm light, respectively. In addition, an emission band at around 703 nm could be resolved in the spectra. Emission was found to be more intensive in suspected area than in healthy tissue. For the healthy tissue maxima around 633 and 703 nm were recorded. Linear unmixing of spectral images from cryoslits was performed using reference spectra of PpIX and mixture of FAD and NADH.

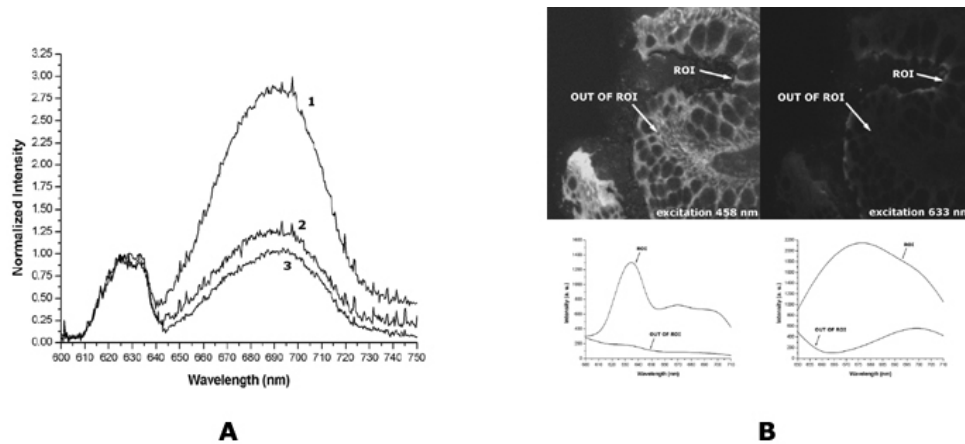


Fig. 1 **A** Fluorescence spectra from suspected area (1), healthy tissue (2) and from suspected area after PDT treatment (3). Excitation was 632.8 nm. **B** Spectral images of cryoslits from suspected area of intestinal tissue. Fluorescence spectra after excitation at 458 nm (left) and 633 nm (right) corresponding to the areas with (ROI) or without (out of ROI) visible red fluorescence are shown below the images.

3. **PDT:** PDT performed 4 hours after ALA administration with red laser giving the total light dose of 48 J/cm^2 resulted in the apparent reduction of superficial precancerous lesions. Each patient had a positive response to therapy. In two cases there was a total response and in other five cases more than sixty percent of suspected area was removed at the time of endoscopic control (one week after PDT treatment). In most of the cases endoscopy showed flattening of the polyps (Figure 2) and appearance of a white necrotic center at the site of the treatment.

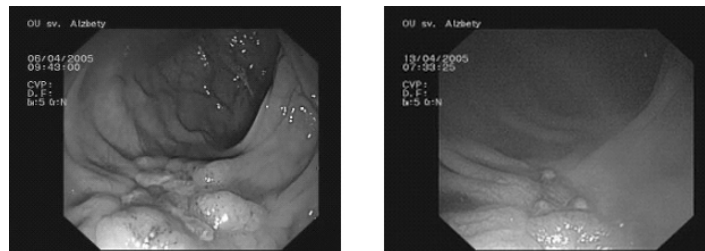


Fig. 2 Endoscopic images of superficial intestinal adenocarcinoma polyps before (left) and one week after (right) PDT

Conclusion: To summarize, differences in fluorescent spectra of PpIX in suspected area and in healthy tissue suggest that this photosensitizer is suitable agent for fluorescence diagnostics of the precancerous tissue. Spectrally resolved fluorescence microscopy gives more detailed picture of accumulation and production of PpIX in tissue. ALA-based PDT is a suitable treatment modality for superficial precancerous lesions of oesophagus and intestine.

Acknowledgement

This work was supported by the research grant from the Slovak Grant Agency Vega 1/2283/05.

References

- [1] D. Nowis, M. Makowski, T. Stoklosa, M. Legat, T. Issat, *Acta Biochimica Polonica*, 52(2) (2005), 339-352.
- [2] A. Ciburis et al., *Experimental Oncology*, 25 (2003), 51-54.
- [3] BC. Wilson et al. *Photochem Photobiol.*, 65 (1997), 166-176.
- [4] S. Andersson, C. Klinteberg, S. Svanberg, *Phys. Med. Biol.*, 42 (1997), 815-824.

UV-VIS absorption and fluorescence investigation of the interactions of hydroxyanthraquinones with human serum albumin

Š. BÁLINT¹, Ľ. BURIANKOVÁ¹, G. FABRICOVÁ¹, D. JANCURA¹ AND P. MIŠKOVSKÝ^{1,2}

¹ Department of Biophysics, P. J. Šafárik University, Jesenná 5, 041 54 Košice, Slovakia.

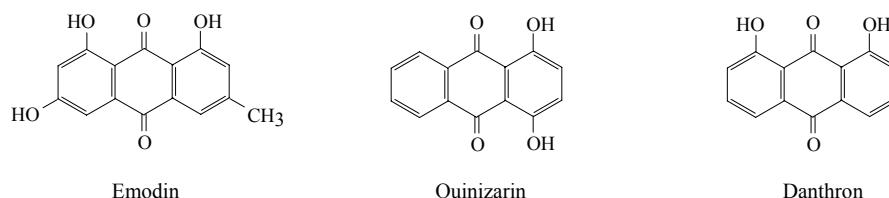
² ILC, Ilkovičova 3, 812 19 Bratislava, Slovakia.

e-mail: balint.stefan@gmail.com

Hydroxyanthraquinones belong to an important class of biologically active and commercially valuable compounds. They are of interest as dyes, pesticides and fungicides as well as additives in lubricants. From biological point of view, molecules of this group possess ability to act as cytotoxic and genotoxic agents as well as the parent molecules for anthracycline antitumor drugs [1, 2]. The interaction of hydroxyanthraquinones with serum proteins (serum albumin, lipoproteins ...) can substantially modify biological activity of these molecules in biological systems.

Serum albumins are the most abundant plasma proteins and contribute significantly to many transport and regulatory processes. The proteins bind a wide variety of substrates such as metals, fatty acids, amino acids, hormones and an impressive spectrum of drugs [3]. Serum albumins are known to contain two specialized drug binding sites located in subdomains IIA and IIIA [3, 4].

In this work, we used UV-VIS absorption and fluorescence spectroscopy to study the interaction of selected hydroxyanthraquinones (emodin, quinizarin, dantron) with human serum albumin (HSA). Based on spectroscopic measurements we determined binding constants and suggested binding sites for individual hydroxyanthraquinones in HSA.



Our results show that quinizarin specifically binds with HSA at molar ratio 1:1 and the binding dissociation constant was determined as $K_d = 1.79 \times 10^{-6}$ M. Formation of quinizarin–HSA complex leads to quenching of the fluorescence of the tryptophan in HSA structure (Trp 214 is located in IIA subdomain), which suggests that quinizarin binds to this subdomain of HSA. Danthron interacts with HSA by binding to two specific sites. The first is characterized by $K_d = 8.54 \times 10^{-7}$ M and the second, weaker, has $K_d = 1.77 \times 10^{-5}$ M. Very similar behavior was observed in the case of emodin, where the binding constants were determined as $K_d = 6.97 \times 10^{-7}$ M and 4.40×10^{-5} M, for the first and the second binding site, respectively. On the basis of the measurement of the quenching of Trp we suppose that the higher affinity site for danthron and emodin is located in the IIA subdomain. For the precise determination of the binding sites of these molecules we will realize competitive experiments with known ligands of IIA (warfarin) and IIIA (diazepam) subdomains.

The obtained results reveal that the number and positions of hydroxyl groups and the presence of methyl group in the structure of hydroxyanthraquinones play important role in the mode of interaction of this type of molecules with HSA.

Acknowledgement

This work was supported by the Slovak Science and Technology Assistance Agency under the contract No. APVV 20-036104, grant No. G-1/2278/05 of the Scientific Grant Agency of the Ministry of Education of Slovak Republic and VVGS grant of P.J. Safarik University in Kosice No. 19/2004

References

- [1] I. Gutierrez, S. Bertolotti, M. Biasutti, A. Soltermann and N. Garcia, *Can. J. Chem.* 75 (1996), 423-428.
- [2] J.W. Lown, *Pharm. Ther.* 60 (1993), 185-214.
- [3] T. Peters, *Adv. Protein Chem.* 37 (1985), 161-245.
- [4] U. Kragh-Hansen, *Mol. Pharmacol.* 34 (1988), 160-171.

Automated text search and analysis tool for mining biological literature

R. DURNÝ AND J. ULIČNÝ

Department of Biophysics, P. J. Šafárik University, Jesenná 5, 041 54 Košice, Slovakia.

The problem of molecular interactions analysis is hindered with great numbers of possible interactions that must be taken into account. Reduction of the number of interesting interactions to most relevant ones is crucial point allowing computationally tractable simulations and dynamics analysis.

The problem of proper recognition of eventual interacting pairs of molecules is very acute in complex processes, e.g. those that participate in apoptosis. While there is no substitute for careful and critical work with literature sources, describing individual interactions which may be of interest, the huge number of scientific papers devoted to apoptosis (over 13000/year) makes traditional work with sources too difficult for any individual or collective. Therefore it is necessary to find an approach to data mining of these information without direct human interaction.

In this contribution we present automatic text processing methods to search biological literature in electronic format to find a potential interaction. This method is based on the measure of proximity of names of characteristic molecules associated usually with apoptosis.

Results of such automated search are presented in a file of potential interaction pairs, accompanied by identification of paper and location containing the description of interaction candidate.

An example of this method is demonstrated on computer analysis of 72 papers from online database <http://medline.cos.com/>, looking for interactions common to both PKC family of proteins and apoptosis. Initial version of the method allows to reduce the number of papers relevant for both classes of interactions by 60%.

Conformational transitions of Poly-L-lysine: A viscosimetric study of aggregation

D. FEDUNOVÁ¹, M. BÁNÓ¹, J. BÄGELOVÁ¹ AND M. ANTALÍK^{1,2}

¹ Institute for Experimental Physics, Slovak Academy of Sciences, Watsonova 47, 040 01 Košice, Slovakia

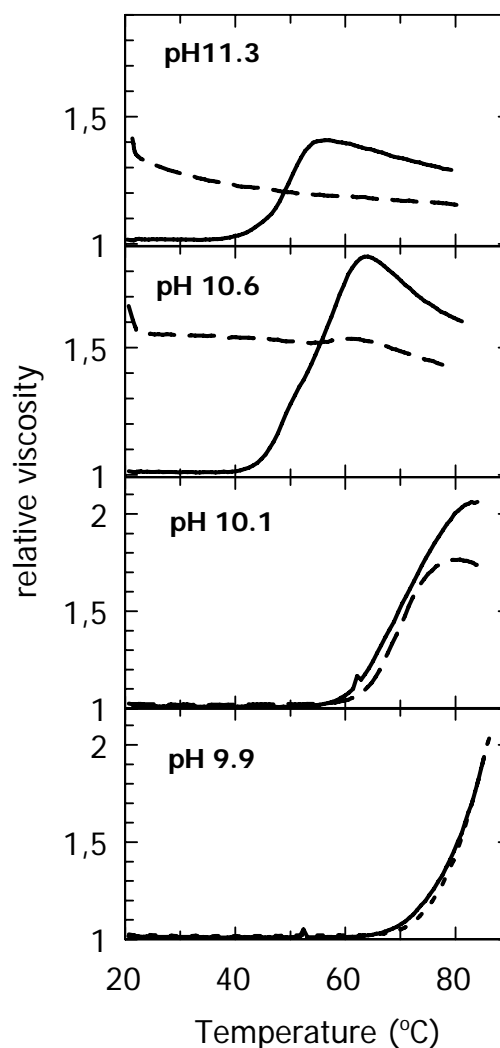
² Department of Biochemistry, P. J. Šafárik University, Moyzesova 11, 040 01, Košice, Slovakia.

e-mail: antalik@saske.sk

The deposition of proteins in the form of amyloid aggregates is the characteristic feature of more than twenty degenerative diseases including known Alzheimer's, Parkinson's and the prion diseases [1]. Although soluble precursors of amyloidogenic proteins do not have any obvious sequence homology of common folding patterns, CD and IR studies indicate that all amyloid fibrils share a characteristic cross- β -structure [2]. β aggregates of polylysine have an amyloid-like outlook in transmission electron microscopy [3].

Recent studies suggest that many peptides and proteins not associated with amyloid diseases possess an intrinsic ability to assemble into amyloid fibrils similar to those observed in disease states under appropriate conditions [4]. Furthermore, it has been indicated that amyloid fibril formation is an evolutionary conserved biological pathway used to generate natural product nanostructures, which have attracted much attention for nanotechnological and material science applications [5]. Although significant research efforts have helped elucidate some features of protein aggregation, comprehensive mechanism remain still elusive. The observed common character of protein aggregation enable to seek further clues by studying generalized sequenceless polypeptide models. One of the most successfully studied model polypeptides is polylysine. This homopolypeptide gains a disordered state at low pH, low ionic strength and ambient temperature, an α -helix at high pH and low temperature and β -sheet at high pH and high temperature [6].

In this work we have studied conformational transitions of poly-L-lysine with different chain length at alkaline pH and various temperatures by means of viscometry and CD spectroscopy. The viscometry seems to be very useful method for study of protein's conformational transitions due to the high sensitivity to the rearrangement of macromolecules in solution. We have used three type of poly-L-lysines differing in chain length (m.w.~1000, ~27000 and ~59 000). We have shown that pK constant of random coil – α -helix transition at room temperature decreases with



Thermal dependence of reduced viscosity at different pH, 0.5 mg/ml poly-L-lysine (Mw ~ 59 000), 10 mM Glycine. Second scan depicted by dashed line at each graph.

increasing of chain length. At alkaline pH polylysine forms α -helical structure. At pH interval from 10.0 to 11.8 temperature induced α -helix to β -sheet transition occurs. The transition temperature decreases with increasing molecular weight of the polypeptide. The increase of chain length is expected to be accompanied by water stabilizing effect on α -helix. However, elongation of a polypeptide chain imply not only elongation of α -helix but brings about higher content of distorted helices with turns enhancing aggregation and leading to the lowering of transition temperature [7]. For each polymer we have observed an increase of transition temperature with decrease of pH. The formation of β -sheet or aggregated structures is hampered by decreasing pH because of electrostatic repulsion, polypeptide chains are kept apart in solution in the random coil. We have also found very narrow pH interval, in which the thermal transition is fully reversible even it appears at high temperatures. Thus, important role in stabilization of α -helix and ability to underlie reversible thermal transition to β -sheet of higher aggregates plays also the amount of charged groups on polymer chain. We have observed slight differences in transition temperatures obtained by viscometry and CD spectroscopy. The CD measurements monitor nature of secondary structure while viscometry is sensitive to formation of higher structures.

Acknowledgement

This work was supported by the research grant from the Slovak Grant Agency Vega No. 4086 and No. 6167. Authors would like to thank Dagmar Sedláková for CD measurements.

References

- [1] J. D. Sipe and A. S. Cohen, *J. Struct. Biol.* 130 (2000), 88-98.
- [2] M. Sunde, L. Serpell, M. Bartlam, P. E. Fraser, M. B. Pepys and C. C. Blake, *J. Mol. Biol.* 273 (1997), 729-739.
- [3] M. Fandrich and C. M. Dobson, *EMBO J.* 21 (2002), 5682-5690.
- [4] M. Fandrich, M. Fletcher and C. M. Dobson, *Nature.* 410 (2001), 165-166.
- [5] J. W. Kelly and W. E. Balch, *J. Cell. Biol.* 161 (2003), 461-463.
- [6] B. Davidson and G. D. Fasman, *Biochemistry.* 6 (1967), 1616-1629.
- [7] W. Dzwolak, T. Muraki, M. Kato and Y. Taniguchi, *Biopolymers.* 73 (2004), 463-469.

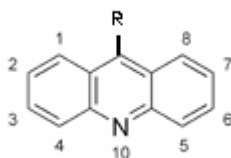
Searching for acridine derivatives with antiaggregating activity and minimal intercalative activity

Z. GAŽOVÁ, J. BÁGELOVÁ AND M. ANTALÍK

Department of Biophysics, Institute of Experimental Physics, Slovak Academy of Sciences, Watsonova 47, 040 01 Košice, Slovakia
e-mail: gazova@saske.sk

The protein deposition diseases, including the prion diseases, Alzheimer's and Parkinson's diseases as well as diabetes type II, involve aggregation of normally soluble proteins or peptides and generation of insoluble amyloid fibrils or plaques [1]. The deposits can be found in the brain, in skeletal tissue or in other organs with a single predominant protein component that is characteristic of each disease. Despite the structural and chemical differences of the amyloid proteins, amyloid fibrils are surprisingly similar in their appearance and structural features. There is a debate on whether fully aggregated protein or smaller precursor (oligomers) cause cellular damage, but emerging evidence indicates that lowering production or removal of aggregates is one pathway alleviating the disease state. Therapeutic strategies targeting these diseases have focused on either increasing the lability of the aggregated state or inhibiting initial oligomerization of the aberrant, misfolded protein [5]. Therefore, identification of inhibitors with disaggregating and/or inhibiting activity plays important role for prevention as well as the therapy of amyloidosis.

Acridines are a special class of compounds due to their possible utility in the pharmaceutical industry. Recently, Quinacrine was identified as a potent inhibitor of PrP^{Sc} formation [2]. Antiprion activity of other acridine and bis-acridine derivatives was reported following their capability to reduce PrP^{Sc} concentration in scrapie-infected neuroblastoma cells [3]. Antiaggregating activity of acridine analogs suggest their utilization as potent inhibitors for the treatment of prion disease. The acridinium derivatives also interact with DNA through intercalation and/or electrostatic modes[4]. This has been exploited in their evaluation as compounds to treat cancer [5,6]. DNA intercalation by acridines, however, leads to a significant modification of the DNA structure and may result in a hindered or suppressed function of the nucleic acid in physiological processes. Separation of desirable bioactivity of these compounds from their DNA intercalative cytotoxicity is important for targeting acridine-based therapy of amyloid diseases.



Chemical structure of acridine derivatives

We focused our efforts to find acridine-based compounds with high protein antiaggregating and minimal intercalative activity. We screen a small library of structurally distinct acridine derivatives with various bulky side groups for their ability to interact with DNA. To investigate how steric and conformational factors influence the mode and extent of acridine binding properties, we used electronic absorbance and fluorescence titrations techniques. The resulting binding isotherms were used to estimate the binding constants and binding size, i.e. the number of occupied binding sites. Complex formation between DNA and

acridine-based compounds was studied also by DSC to obtain thermodynamic profile of interaction.

From these screens we have demonstrated that by introducing subtle steric factors one may alter the DNA binding properties of acridine derivatives. We found out that a formation acridine-DNA complex is affected not only by planar intercalating template, but also by the composition and structure of side chain.

Acknowledgement

This work was supported by research grants from the Slovak Grant Agency Vega No. 6167 and No. 4068. We thank Prof. P. Kristian and Prof. J. Imrich for the acridine derivatives.

References

- [1] M. Bucciatti, E. Giannoni, F. Chiti, F. Baroni, L. Formigli, J. Zurdo, N. Taddei, G. Ramponi, C. M. Dobson and M. Stefani, *Nature* 416 (2002), 507-511.
- [2] K. Doh-Ura, T. Iwaki and B. Caughey, *J. Virol.* 74 (2000), 4894-4897.
- [3] B. C. H. May, A. T. Fafarman, S. B. Hong, M. Rogers, L. W. Deady, S. B. Prusiner and F. E. Cohen, *PNAS* 100 (2003), 3416-3421.
- [4] J. C. Sacchettini and J. W. Kelly, *Nat. Rev. Drug. Discov.* 1 (2002), 267-275.
- [5] T. K. Chen, R. Fico and E. S. Canellakis, *J. Med. Chem.* 21 (1978), 868-874.
- [6] J. B. Hansen, E. Langvad, F. Frandsen and O. Buchardt, *J. Med. Chem.* 26 (1983), 1510-1514.

The influence of selected derivatives of anthraquinones on DNA structure

V. HAVRILOVÁ¹, J. ADAMČÍK², G. FABRICIOVÁ¹, D. JANCURA¹, P. DANKO², M. REFREGIERS³, D. CHORVÁT, JR.⁴
AND P. MIŠKOVSKÝ^{1,4}

¹ Department of Biophysics, Faculty of Natural Sciences UPJS, Jesenna 5, 041 54 Kosice, Slovakia

² Department of Biochemistry, Faculty of Natural Sciences UPJS, Moyzesova 11, 041 54 Košice, Slovakia

³ Centre of Molecular Biophysics, rue Charles-Sadron, 450 71 Orleans Cedex 2, France

⁴ International Laser Centrum, Ilkovicova 3, 812 19 Bratislava, Slovakia

e-mail: havrilv@kosice.upjs.sk

Significant progress has been made over the past few years in studies of drug-DNA interactions. Structure-based design strategies have yielded new DNA-binding agents with clinical promise. Many small molecules that bind to DNA are clinically proven therapeutic agents, although their exact mode of action remains incompletely defined.

Dihydroxyanthraquinones are planar, aromatic molecules. These molecules have important application as a prominent family of pharmaceutically active and biologically relevant chromophores, as an analytical tool for the determination of metals, and in many aspects of electrochemistry [1]. Danthron (1,8-dihydroxyanthraquinone) and quinizarin (1,4-dihydroxyanthraquinone) are the simplest molecules showing the chromophore framework peculiar to several compounds of biological and pharmaceutical interest. The former is present in some antitumor drugs as hypericin, aclacinomycin, emodin and the latter in doxorubicin, daunorubicin and adriamycin [2-4].

Two broad classes of noncovalent DNA-binding agents have been identified, the intercalators and the groove binders. Intercalators bind by inserting a planar aromatic chromophore between adjacent DNA base pairs, whereas groove binders fit into the DNA minor groove causing little perturbation of the DNA structure [5].

In this work we study the interaction of chosen derivatives of anthraquinones quinizarin and danthron with plasmid and linear DNA. To study of the effect of danthron and quinizarin to structure of DNA were employed gel electrophoresis, temperature gradient gel electrophoresis (TGGE) and atomic force microscopy (AFM). Results of electrophoretic experiments revealed that danthron and quinizarin interact with DNA and allow us to suggest that both dihydroxyanthraquinones intercalated into the DNA. The results of AFM and TGGE measurements support this interpretation. The properties of complexes both derivatives of anthraquinones with DNA were also studied by means of optical spectroscopy, i.e. fluorescence and surface-enhanced Raman spectroscopy.

Acknowledgement

This work was supported by the Slovak Science and Technology Assistance Agency under the contract No. APVT-20-036104. The authors wish to thank Mrs. Francoise Culard from Centre of Molecular Biophysics in Orleans, France for many stimulating discussions and providing of experimental conditions.

References

- [1] J. P. Brown, *Mutation Research* 75 (1980), 243-277.
- [2] R. H. Thomson, *Naturally Occurring Quinones* (1971), Academic Press, New York.
- [3] Y. Nonaka, M. Tsuboi, K. Nakamoto, *J Raman Spectrosc.* 21 (1990), 133.
- [4] D. Jancura, S. Sanchez-Cortes, E. Kocisova, A. Tinti, P. Miskovsky, A. Bertoluzza, *Biospectroscopy* 1 (1995), 265.
- [5] S. S. Hall, *New York Times Magazine* 147 (1997), 64-71.

Internalization mechanisms of hypericin in glioma cell line U-87 MG studied by fluorescence spectroscopy and microscopy

S. KAŠČÁKOVÁ^{1,2}, M. REFREGIERS^{2,3}, D. JANCURA¹, A. MATEAŠIK⁴, V. HUNTOŠOVÁ¹, J.-C. MAURIZOT² AND P. MIŠKOVSKÝ^{1,4}

¹ Department of Biophysics, P.J. Safarik University, Kosice, Slovakia

² Centre de Biophysique Moleculaire, CNRS UPR4301, Orleans, France

³ Synchrotron SOLEIL, Gif sur Yvette, France

⁴ International Laser Center, Bratislava, Slovakia

The incorporation and subcellular localization of photosensitizers (pts) are critical determinants of their efficiency in photodynamic therapy of cancer (PDT). Serum proteins are mainly responsible for the transport of drugs into the different parts of the human body, including tumor tissue. The binding of anti-cancer drug, including pts, to the various types of serum proteins is mainly governed by the degree of hydrophilicity/lipophilicity [1-5]. Probably, the most important natural transporters of hydrophobic photosensitizers to tumor tissue are the low-density lipoproteins (LDL) [6, 7].

The development of new-generation of pts to improve PDT as well as photodynamic diagnosis is an area of extensive research. One of the most promising pts in PDT appears to be hypericin (Hyp). Hyp is a natural photosensitizing agent occurring in plants of the genus *Hypericum*, which under illumination displays an virucidal activity as well as antiproliferative and cytotoxic effect on tumor cells [8, 9].

Using methods of fluorescence spectroscopy and microscopy we have investigated the uptake and the internalization mechanisms of Hyp in glioma cell line U-87 MG as the function of the presence of different transport serum proteins in cultivation medium (human serum albumin (HSA), LDL, 10 % serum enriched medium and depleted medium). The results show, that the accumulation of Hyp by U-87 MG in the presence of LDL is proportional to the Hyp/LDL molar ratio. This indicates that the amount and aggregation state of Hyp inside LDL [10] do not influence the ability of LDL to be internalized into cells.

Uptake of LDL by cells is realized by the specific receptor endocytosis pathway. We have shown that activation of LDL receptors leads to substantial increase of Hyp uptake by U-87 MG in the presence of LDL. It means that LDL particles seem to be effective transporters of hydrophobic Hyp to cells through LDL receptor pathway.

It was demonstrated that internalisation of Hyp into U-87 MG cell line seems to be the result of different mechanisms depending on the composition of the cultivation medium. We detected differences in the intracellular concentration of Hyp as well as in the time of maximum of the uptake in the presence of different serum proteins in the medium. These observations are important from the point of view of possible application of Hyp in PDT.

Acknowledgement

This work was supported by the Slovak Science and Technology Assistance Agency under the contract APVT-20-036104, by the Scientific Grant Agency of the Ministry of Education of Slovak Republic under the grant 1/2278/05 and by the contract 2003/4837 of the French Government (cotutoring doctoral thesis of S.K.).

References

- [1] A. N. L. Derycke, P. de Witte, *Adv. Drug Deliver. Rev.* 56 (2004), 17-30.
- [2] G. Jori, *J. Photoch. Photobiol. B.* 36 (1996), 87-93.
- [3] Y. N. Konan, R. Gurny, E. Alleman, *J. Photoch. Photobiol. B.* 66 (2002), 89-106.
- [4] E. Reddi, *J. Photoch. Photobiol. B.* 37 (1997), 189-195.
- [5] W. M. Sherman, J.E. van Lier and C. M. Allen, *Adv. Drug Deliver. Rev.* 56 (2004), 53-76.
- [6] L. Polo, G. Valduga, G. Jori and E. Reddi, *Inter. J. Biochem. & Cell Biol.* 34 (2002), 10-23.

- [7] S. Bonneau, C. Vever-Bizet, P. Morliere, J.C. Maziere and D. Brault, *Biophysical Journal* 83 (2002), 3470-3481.
- [8] P. Miskovsky, *Current Drug Targets* 3 (2002), 55-84.
- [9] P. Agostinis, A. Vantieghem, W. Merlevede and P. de Witte, *Inter. J. Biochem. & Cell Biol.* 34, (2002) 221-241.
- [10] S. Kascakova, M. Refregiers, D. Jancura, F. Sureau, J.-C. Maurizot and P. Miskovsky, *Photochemistry and Photobiology* 81 (6) (2005), 1395-1403.

The new Raman facility of the International Laser Center in Bratislava

Š. BÁLINT¹, Cs. BÍRÓ², G. LAJOŠ¹ AND P. MIŠKOVSKÝ^{1,3}

¹ Department of Biophysics, P. J. Šafárik University, Jesenná 5, 041 54 Košice, Slovakia.

² Department of Biophysics, Faculty of mathematics, physics and informatics, Comenius University, 842 48 Bratislava, Slovakia.

³ International Laser Centre, Ilkovičova 3, 812 19 Bratislava, Slovakia.
e-mail: miskovsky@ilc.sk

A newly established Raman facility of the International Laser Center in Bratislava is presented. The laboratory consists of two independent installations: macro- and micro-Raman setups.

Macro-Raman setup: Triple monochromator system *TriVista*[®]System (Princeton Instruments, Acton Research Corp., USA; comprising of three motorized SpectraPro 2500i spectrographs with focal distance 500mm) working in subtractive and additive modes in UV-VIS region (~240-700nm). The last monochromator stage is equipped with Spec-10 (Princeton Instruments, Roper Scientific Inc., USA,) thermoelectrically cooled CCD camera with 2048x512 chip (e2v technologies Ltd., UK). In addition to triple modes, a direct access to the 3rd stage spectrograph is available through appropriate notch filters, allowing to measure low-intensity samples such as low-volumes of diluted biological macromolecules in solutions. Excitations wavelengths are generated by Ar⁺-ion laser FreD90C (Coherent, USA) with the intra-cavity frequency doubler crystals providing three UV lines (257-, 244- and 228 nm). Other lasers, such as the tunable nanosecond OPO pumped by the third harmonic of the Nd:YAG laser (both Solar, Belarus), or pulsed DPSS YAG lasers (LaserCompact, Russia) are available for the time-resolved studies, providing the excitation range of ~350-2000nm.

Micro-Raman setup: Micro-Raman setup is based on Axiovert 200M motorized inverted microscope (Zeiss, Germany), combined with the imaging monochromator *SpectraPro 300i* (Princeton Instruments, Acton Research Corp., USA; focal distance 0,300m). The spectrograph is attached to the microscope through the notch-filter assembly with the notch filter corresponding to the 785nm NIR laser diode (Renishaw plc., UK) used as an excitation source. The monochromator is equipped with the second Spec-10 (Princeton Instruments, Roper Scientific Inc., USA,) TE-cooled CCD camera with 1340x400 chip. In addition to Raman mode, the microscope is equipped also with halogen and mercury lamps. Thus, the system can be used for both Raman and fluorescence spectroscopy / imaging applications on the same sample. In order to provide controlled physiological conditions of biological samples, such as cells or tissues, a CO₂/O₂ incubator with temperature conditioning system (PeCon/LaCon, Germany) and mercury-lamp illumination control (FluoArc, Zeiss, Germany) attenuating the light intensity in the range of 20-100% of the HBO lamp power is provided.

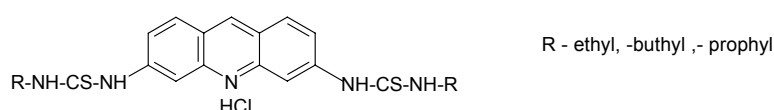
Interaction of proflavine derivatives with nucleic acid

D. SABOLOVÁ, M. KOŽURKOVÁ, J. SABOVÁ AND D. PODHRADSKÝ

Institut of Chemistry, Department of Biochemistry, faculty of Sciences UPJŠ, Košice

Proflavine is an acriflavine derivative which is a disinfectant bacteriostatic against many gram-positive bacteria. It is toxic and carcinogenic in mammals. It has been widely assumed that the proflavine act primarily on nucleic acids. The concept of interaction with DNA through intercalation was first demonstrated with proflavine [1] and later with other acridines. The development of new compounds which modify nucleic acid structure is a current research area and can make a significant contribution to anti-tumor and anti-viral chemotherapy [2,3].

In present work the intercalation of new proflavine dithioisoureas (*PDs*) (Scheme 1) into plasmid pUC 19 has been studied.



Scheme 1 Structure of proflavine dithioisoureas hydrochlorides (PD-ethyl, PD-propyl, PD-butyl)

The absorption spectrum of proflavine derivatives with DNA measured in 0.1 M Tris buffer exhibited a broad absorption of high resolution in the regions 325–425 nm and 260–325 nm.

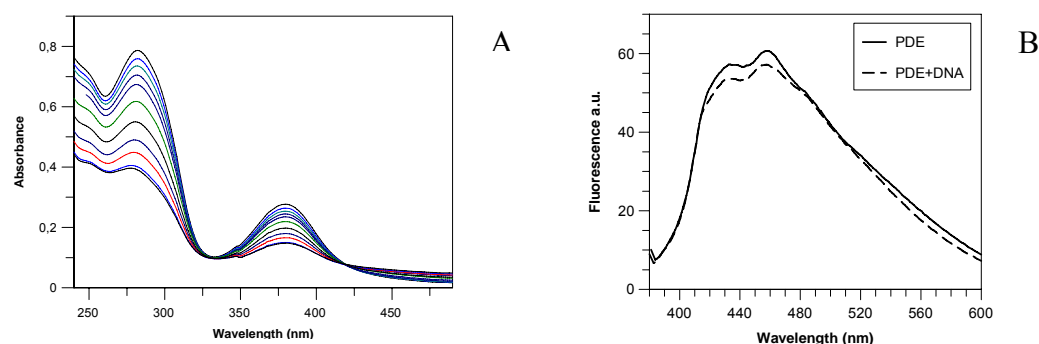


Fig. 1 UV-vis titration spectra (A) and fluorescence emission spectra (B) of PD-ethyl (2.6×10^{-6} M) with pUC 19 DNA (6.3 μ M bp) measured in 0.1 M Tris buffer (pH=7.4)

Fig. 1A provides an example illustration the characteristic changes during UV-vis titration of PD-ethyl with pUC 19. The addition of DNA to the solution of PD-ethyl resulted in a slight decrease in the absorption of the acridinium chromophore. The absorption bands were shifted to a longer wavelength with the isosbestic point at 417 nm. Fig. 1B illustrates the fluorescence emission spectra of **PD-ethyl** in the absence (solid line) and presence (dashed line) of pUC 19 after exciting it at 365 nm.

The absorbance quenching experiments were analyzed to construct binding isotherms [4]. The binding constants of PDs with DNA were estimated from the titration curves by the model of McGhee and von Hippel using Grafit 4 software (Table 1).

Tab. 1 Binding parameters of DNA-PDs complexes

Compound	PD-ethyl	PD-propyl	PD-butyl
binding constant K (M⁻¹)	2.6x10 ⁵	2.8x10 ⁵	2.9x10 ⁵

The UV-vis absorption and fluorescence emission spectra suggest that new proflavine compounds interact with DNA by intercalation. The obtained results support the idea that intercalative π -stacking interactions of the ligands with DNA are essential for observing their efficient electron transfer reaction.

Acknowledgement

This work was supported by the research grant from the Slovak Grant Agency Vega No. 1/1272/04 and 1/1274/04.

References

- [1] M.J. Wainwright, *J. Antimicrob. Chemother.* 47 (2001), 1-13.
- [2] B. Baldeyrou, C. Tardy, C. Bailly, P. Colson, C. Houssier, F. Charmantray, M. Demeunynck, *Eur. J. Med. Chem.* 4 (2002), 315-22.
- [3] J. Joseph, E. Kuruvilla, A. T. Achuthan, D. Ramaiah, G. B. Schuster., *Bioconjug. Chem.* 15 (2004) 1230-1235.
- [4] T.C. Jenkins in *Methods in molecular biology*, Vol. 90 Part Drug-DNA interaction protocols K.R. Fogs (Ed.) Humana Press Inc., Totowa, NJ (1997).

Determination of solvation structures of various ionic forms of naphthazarin in water, DMSO and water/DMSO mixtures.

M. SAVKO, S. KAŠČÁKOVÁ, D. JANCURA AND J. ULIČNÝ

Department of Biophysics, Faculty of Natural Sciences UPJŠ, Košice

The interest for naphthazarin (NZ) (fig.1) is due to its biologically relevant properties (antimicrobial activity, can induce apoptosis ...) [1][2] shared with other quinone derivatives which are often to be referred to as potent antiviral and antitumoral agents (warfarin, hypericin, daunomycin, andriamycin, tricozarin B).

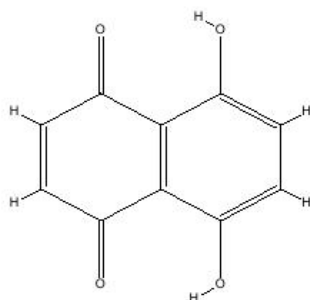


Fig. 1 Structural formula of naphthazarin

The determination of acid dissociation constants, important parameters to define the extent of ionization of drug molecules at different pH values, is often required in various chemical and biochemical applications. During the determination of acid dissociation constants of NZ by means of emission spectroscopy an unexpectedly strong emission at 518 nm was observed in solution with pH over 9 (region of wavelengths and pH for which only low absorption is being detected).

To validate some of hypothesis explaining this phenomenon by effects of solvation and/or aggregates formation we have performed set of molecular dynamics (MD), simulations in relevant solutions: water, DMSO and mixtures of water and DMSO with molar ratios 1:3 and 1:1. (DMSO solutions were included to reflect the fact that experiments were made in water solution with certain amount of DMSO added to increase solubility of NZ, what induces some questions with respect to known special properties of water/DMSO mixtures [4]). Simulations were performed for monomers as well as for dimers of various relevant forms of NZ (neutral, monoanionic and dianionic) in NPT ensemble with normal pressure and temperature 303 K.

Statistical analysis of MD trajectories revealed creation of local solvation structure around individual NZ molecules. This can be clearly seen in RDF figures (fig. 2). Stability of local solvation structures increases for deprotonated forms for all studied solvents.

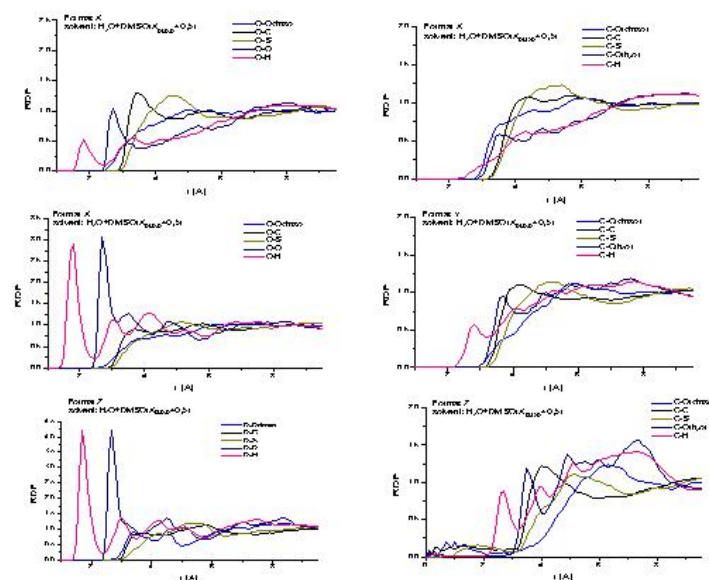


Fig. 2 RDFs of NZ protomers

The most significant strengthening of local structure (described in terms of hydrogen bonds and contacts creation and persistence) is being observed in mixture of water and DMSO with 3:1 molar ratio, which is in an correlation with reported [4] very interesting behavior of physico-chemical properties with respect to water/DMSO ratio in water/DMSO mixtures (many of these properties attains their maximal or minimal values at molar ratio of DMSO in proximity of 0.25).

This leads us to the conclusion that electronic spectra could reflect effective concentration which is not the same that apparent macroscopic concentration. In other words there is a preference of NZ molecules to create more less persistent complexes with DMSO and water. And these complexes make statistically dominant configuration for absorption-emission characteristics. In order to identify the most important configurations for such analysis we have performed careful trajectory analysis using rigid body approach, which permitted us to describe relative positions of NZ and solvent molecules using six independent coordinates (parameters). We identified the most important configurations which will serve in further investigation using methods of quantum molecular theory to determine respective impact of distinct salvation structure on electronically excited states properties.

Acknowledgement

This work was supported by the VVGS grant of P.J. Safarik University in Kosice No. 215/2005.

References

- [1] M. Moir, R.H. Thomson, *Phytochemistry* 12 (1973) 1351.
- [2] A. Ohta, P.M. Sivalingham, S. Lin, N. Ikekawa, N. Yaginuma, Y. Inada, *Toxicon* 11 (1973) 235-241.
- [3] P.M. Rentzepis, V.E. Bondybey, *J. Chem. Phys.* 80, 4727, 1984.
- [4] A. Vishnyakov, A. Lyubartsev and A. Laaksonen, *J. Phys. Chem. A*, 105, 1702-1710, 2001.
- [5] W. L. Jorgensen, D. S. Maxwell and J. Tirado-Rives, *J. Am. Chem. Soc.*, 117, 11225-11236, 1996.
- [6] Y.H. Mariam, R. Musin, *J. Mol. Structure: THEOCHEM* 586(1-2), 123, 2001.
- [7] U.C.Singh, P.A.Kollman, *J. Comput. Chem.*, 14, 1504-1518.
- [8] Tinker, *Software Tools for Molecular Design*, Version 4.2, June 2004; dasher.wustl.edu/tinker

Role of polypeptide chain dynamics for conformational isomerization and ligand binding. Cytochrome *c* study.

N. TOMÁŠKOVÁ¹, R. VARHAČ², L. VARINSKÁ¹, G. ŽOLDÁK¹, D. SEDLÁKOVÁ² AND E. SEDLÁK¹

¹Department of Biochemistry, Faculty of Natural Sciences UPJŠ, Košice, Slovakia

²Institute of Experimental Physics SAS, Košice, Slovakia

The native conformation of an enzyme is produced by the complex interaction of van der Waals interactions, hydrogen bonds and ionic interactions. These interactions produce stability of the enzyme under physiological conditions and prevent deleterious conformational changes from perturbations in the environment that would cause deactivation. Modulation of the balance between the rigidity and flexibility of the polypeptide and side chains can be achieved by changing the solvent properties. We have shown recently that modulation of polypeptide dynamics of NADH oxidase by chaotropic (urea, Hofmeister series anions) or kosmotropic (Hofmeister series cations) agent leads both to its activation and inhibition [1, 2].

We were interested in how conformational dynamics affects: (i) conformational change and (ii) binding of small ligands. Suitable object for such studies is small globular heme protein mitochondrial cytochrome *c*.

Cytochrome *c* sensitively reacts on solvent pH. Ferricytochrome *c* (cyt *c*) exists in five distinct spectroscopic forms, states I-V, between pH 1 and 12 [3]. State III dominates near neutral pH and is regarded as the native conformation of the protein. Despite the extended time elapsed, elucidation of the structural changes that the cytochrome undergoes as a function of pH has been surprisingly elusive. In the past 30 years, particular attention has been directed towards the characterization of the conformational change that occurs upon titration of mitochondrial forms of cyt *c* from neutral (state III) to alkaline (state IV) pH ($pK_a \sim 8.5-9.5$, depending on species from which the cyt *c* originates and the solution conditions). Reduction potential of alkaline cyt *c* is nearly 0.5 V lower than that of the native cytochrome. This dramatic effect of pH on the fundamental functional property of this small and relatively simple protein makes a structure-based understanding of the origin of this effect of particular effect [4, 5].

The easiest way to follow alkaline isomerization is spectroscopic studies in Soret region. From spectroscopic studies, it was established that conversion of native cyt *c* to the alkaline conformational state results in the disruption of the Met80-Fe bond with concomitant introduction of a new axial ligand to the heme iron that is probably provided by one of the many lysyl residues present on the surface of the protein. Position of lysyl residues suggests a relatively large conformational change in alkaline isomerization. There is a fundamental question if conformational transition as alkaline isomerization is affected by modification of flexibility of polypeptide chain. Polypeptide chain

dynamics of cyt *c* was changed by the anions of Hofmeister series: Cl^- , Br^- , SCN^- and ClO_4^- based on our recent work [2] and monitored by binding rate of cyanide into heme iron and bleaching of heme by hydrogen peroxide. Our results showed that there is

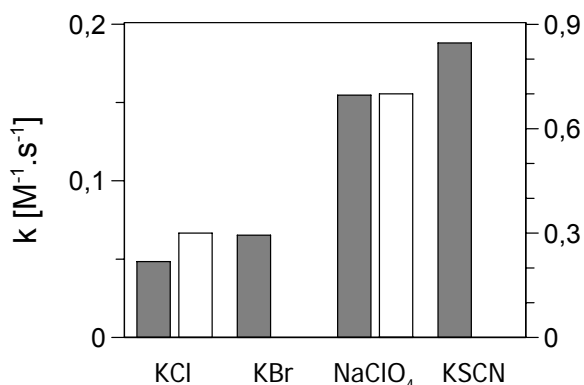


Fig. 1 Effect of anions on rate of cyanide binding (grey bars) and rate of bleaching by hydrogen peroxide (empty bars).

a close correlation between position of anions in Hofmeister serie and (i) rate constant of cyanide binding, k_{CN} (Fig. 1), (ii) $\text{p}K_{\text{a}}$ value of alkaline isomerization (Fig. 2), and (iii) energy characterizing stability of cyt *c*.

This is an interesting result indicating the role of polypeptide dynamics in conformational change of proteins. Our finding also indirectly explains observations that apparent $\text{p}K_{\text{a}}$ of alkaline isomerization can be significantly shifted to higher pH by immobilization of surface accessible lysyl residues by polyanions [6].

Acknowledgements.

This work was supported by the research grants from the Slovak Grant Agency VEGA No. 1/1272/04.

References

- [1] G. Žoldák, R. Šuťák, M. Antalík, M. Sprinzl and E. Sedlák, *Eur. J. Biochem.* 270 (2003), 4887-4897.
- [2] G. Žoldák, M. Sprinzl and E. Sedlák, *Eur. J. Biochem.* 271 (2004), 48-57.
- [3] H. Theorell and A. Åkesson, *J. Am. Chem. Soc.* 63 (1941), 1804-1811.
- [4] F.I. Rosell, J.C. Ferrer, and A.G. Mauk, *J. Am. Chem. Soc.* 120 (1998), 11234-11245.
- [5] L.A. Davis, A. Schejter and G.P. Hess, *J. Biol. Chem.* 249 (1974), 2624-2632.
- [6] M. Antalík, M. Bona and J. Bagelova, *Biochem. Int.* 28 (1992), 675-682.

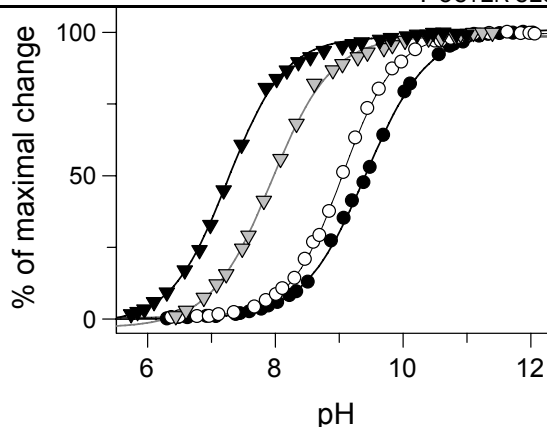


Fig. 1 Effect of anions: chloride (black circles), bromide (white circles), rodanide (grey triangles) and perchlorate (black triangles) on $\text{p}K_{\text{a}}$ value of alkaline isomerization of ferricyt *c* followed in Soret region of its electronic absorption spectrum.

Correlation between UV-induced peroxidation and permeability of liposomes

K.SCHRONEROVÁ AND M. BABINCOVÁ

Department of Nuclear Physics and Biophysics, FMFI Comenius University, Mlynská dolina F1, 842 48 Bratislava 4, Slovakia.

Introduction: Liposomes are often used as model membrane systems to study the effects of different physical or chemical agents on membrane properties, such as fluidity or permeability. Changes in permeability can be caused by, for example, aggregation, fusion or UV radiation. UV radiation induce peroxidation process, that causes the damaging of membrane and change its biophysical properties. Oxidation process can be initiated by reactive oxygen species, such as the superoxide anion O_2^- , hydroxyl radical $\cdot OH$ or singlet oxygen 1O_2 [1,2]. We have chosen doxorubicin as a model drug to find out efficiency of encapsulation drug into liposomes, drug retention and release. This anthracycline antibiotic is one of the most widely used anticancer agents. Doxorubicin, isolated from *Streptomyces peuceutius*, intercalates between adjacent base pairs of the DNA double helix. DOX has antimicrobial activity in addition to his antineoplastic activity [3,4]. Arsenazo, a metallochromic dye, was also encapsulated into liposomes to compare extent of release with doxorubicin. Spectral characteristic of the arsenazo III change markedly in the presence and absence of calcium ions [5]. Calcium binds strongly to the dye and produces a spectral shift from 560nm to 606/660nm, that is a change from red to blue which is a clearly noticeable by eye.

Material and methods : Liposomes of phosphatidylcholine were prepared by thin-film hydrated method. After evaporation of the solvent, aqueous solution of doxorubicin (or arsenazo) was added in desired concentration to the glass vessel with lipid film. The solution was shaken up mechanically. Liposomes with encapsulated doxorubicin were separated from non-encapsulated drug by centrifugation (12000g). The efficiency of encapsulation of doxorubicin (or arsenazo) into liposomes was determined by measuring the transmittance of supernatant and calibration curve. Peroxidative process was initiated by ultraviolet radiation UVA with wavelength range λ (320nm-400nm). Liposomes were exposed to UVA radiation for different period (0-105 min). After irradiation, the leakage of liposomes was studied by measuring the transmittance of supernatant. Lipid peroxidation was monitored by measurement of absorption spectra of conjugated dienes in the wavelength range λ (215nm-320nm) using UV VIS spectrophotometer.

Results and discussion : UV radiation caused the disruption of the membrane of liposomes. As reported earlier, the extent of peroxidation may vary dependly on the time of irradiation. Lipid-bilayer damage increased with increasing irradiation time. The encapsulated cytostatic release from liposomes according to UV-mediated membrane damage (Fig. 1). The maximal release for irradiation time 105 min is for doxorubicin 88,2%. We have also studied the extent of encapsulation and release of dye arsenazo III. As can be seen in Fig. 2, increasing irradiation time leads to the

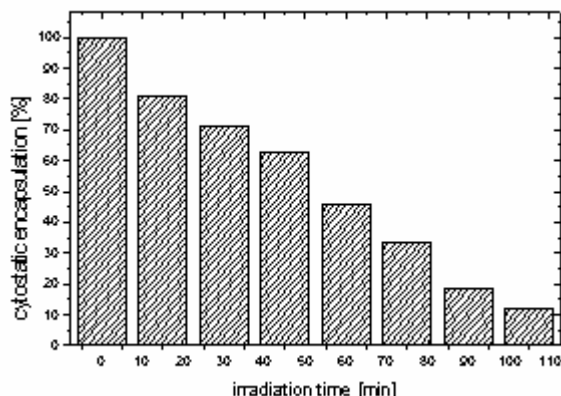


Fig. 1 Dependence of doxorubicin release from liposomes.

decrease of percentage of encapsulated arsenazo. But maximal release for period 105 min is 53,3%.

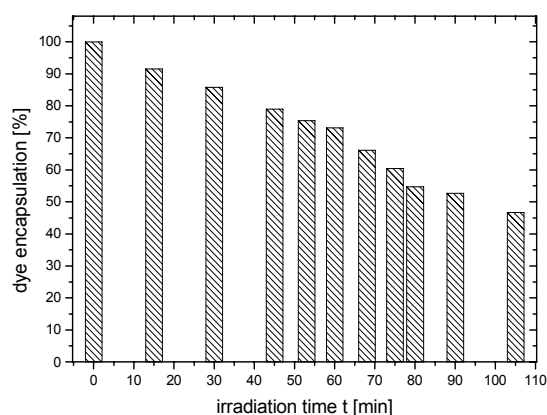


Fig. 2 Extent of Arsenazo III release from liposomes.

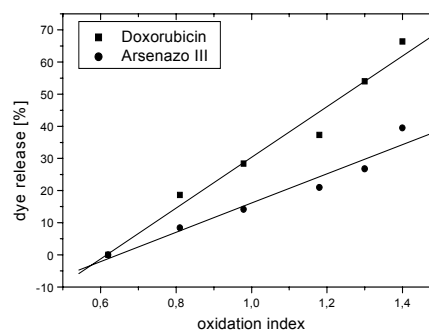


Fig. 3 Correlation between peroxidation process and encapsulated dye release.

Fig. 3. demonstrate a correlation between increase in peroxidation process and the increase in dye release. The results show that there is linear relationship between UV radiation and changes in liposome permeability. It is interesting to note that similar behavior has been found also for the interaction of microwaves with liposomes [6,7]. In this study we have demonstrated that UV radiation induce the peroxidation process in lipid-bilayer. This process caused the structural changes in liposomes, degradation the lipidic molecules and changes in bilayer permability, even after exposure the liposomes to UV for a period 15 min. Irradiated vesicles showed an increased damage upon exposure to UV radiation, which leads to the release of encapsulated drug (or dye) in liposomes. The observed effects indicate that not only damage of DNA is induced by UVA, but also cell membrane may be a target adverse effect of UVA e.g. after prolonged exposure of skin to sun radiation. On the other hand, UV radiation can be used for controlled drug release, e.g. in the treatment of skin tumors.

Acknowledgement

This work was supported by the research grant from the Slovak Grant Agency Vega No. 1/2012/05

References

- [1] H. Trommer, J. Wagner, H. Graener, R.H.M. Neubert, *European Journal of Pharmaceutics and Biopharmaceutics* 51 (2001), 207-214
- [2] M. P. Popova., CH. S. Popov, *Z. Naturforsch.* 57c (2002), 361-365
- [3] F. M. Muggia, *Curr. Oncol. Rep.* 3 (2001), 156-62
- [4] A. Gabison, D. Goren, R. Cohen, Y. Barenholtz, *J. Control Release* 53 (1998), (1- 3): 275-9
- [5] G. Weissmann, T. Collins, A. Evers, Ph. Dunham, *Proc.Nat.Acad.Sci. USA* Vol.73 (1976) 510-514
- [6] M.Babincová, *Z. Naturforsch.* 49c (1994), p.124
- [7] M.Babincová, *Pharmazie* 50 (1995), 702

Combinative therapy, chemotherapy and hyperthermia, used Gleevec – magnetosomes for the treatment of tumors

B.TENCEROVÁ AND M. BABINCOVÁ

Department of Biophysics and Nuclear physics, Faculty of Mathematics, Physics and Informatics, Comenius University, Bratislava, Slovakia

Magnetic fluid and magnetic nanoparticles represent an interesting material both present in areas of technology and useable for variety medical application. We study utilization of new magnetic fluid in combinative therapy of malignant tumors.

Introduction

With an applied uniform time varying field, the particles align in the direction of the field, magnetizing the fluid. After a magnetizing field is switched off, they are returning through two relaxation mechanisms [1]. First Brownian relaxation mechanism, i.e. the entire particle rotates in the surrounding fluid. The second mechanism is Néel relaxation, i.e. the magnetization rotates within the magnetic core. This mechanisms and viscous drag effects are mainly accountable for the heating of ferro-fluids due to power dissipation

Magnetic-fluids have been investigated as potential hyperthermia causing agents due to their high specific absorption rate. The particles will heat up and conduct the heat to the tumor cells, there for hyperthermia is a promising approach for cancer treatment [2]. It has been found that the viability of cancer cells is reduced when the human or animal malignant cells are heated to temperatures between 41–46°C, consecutively their sensitivity to chemotherapy and radiation increase.

Magnetic nanoparticles as vehicles for delivery of anticancer drugs after introduction to the tumor answer for increase of the efficacy and drug concentration at the tumor site, reduce the unpleasant side effects associated with chemotherapy [3,4].

The aim of the study was to prove higher effectiveness of combinative treatment in comparison with single chemotherapy or hyperthermia, at in vitro study on tumor cells and in vivo study on laboratory rat from Sprague dawley lineage.

Material and Methods

Tested ferrofluids is new kind of synthetic aqueous - based magnetic fluids consist of nano-sized iron oxide particles Fe₃O₄ (magnetit), which are suspended in carrier liquid by their thermal energy. Diameter of magnetit core is 30nm. Magnetit particles are coated by polysaccharide surfactant, which creates net repulsion between them and stabilized colloid.

Complex of chemotherapeutic drug adsorbed on nanoparticles is called Gleevec-magnetosom. Gleevec (Imatinib mesilate) is a protein-tyrosine kinase inhibitor that potently inhibits the Bcr-Abl tyrosine kinase as well as the receptors for platelet-derived growth factor (PDGF), stem cell factor (SCF) and c-Kit receptor, at in vitro and cellular kinase assay levels. It inhibits proliferation and induces apoptosis of variety Bcr-Abl, c-Kit positive cells [5,6].

Heating is realized on experimental setup for the generation of an alternating magnetic field with frequency of 3,5 MHz and induction of 1,5 mT produced in three-turn pancake coil cooled with water. Temperature inside suspension was measured using nonabsorbing thermistor.

Results and Discussion

Fig.1 shows extent of three ferrofluids heat-up, containing various concentrations of magnetit particles, under influence of alternating magnetic field. Heating of ferrofluids is due to the relaxations mechanism and viscous drag effects. As can be seen, the highest increase of temperature is observed at the fluid with highest concentration of magnetit particles, lower time of magnetization. Therapeutic temperature 44°C was achieved in every pattern in the time: 80 mg/ml in 8 min, 24 mg/ml in 25 min, 16 mg/ml in 40 min.

In Fig.2 we compare efficiency of single therapies. Look at the higher complex of columns. Highest percentage of tumor cells decrease was observed at combinative therapy 75%, where we used maximal concentration of Gleevec adsorbed on definite quantity of magnetit nanoparticles. With chemotherapy we observed 55% and with hyperthermia 20%. In our experiments we have demonstrated that combinative therapy is from these the most suitable for treatment.

In the conclusion it is important to note, that the tested ferrofluid with magnetit particles qualified to fit the means of combinative therapy, what we can see in Fig. 2, that combinative therapy realized by Gleevec-magnetosomes in time varying field is more efficient than hyperthermia realized by magnetit particles and than chemotherapy realized by Gleevec.

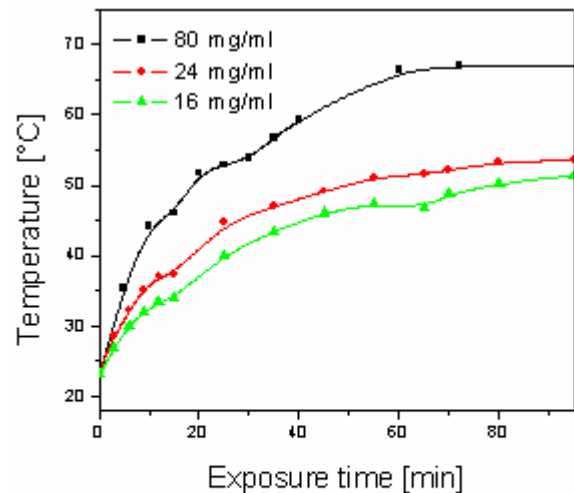


Fig.1. Dependence of magnetic-fluid heating from various concentration of magnetit nanoparticles. The results are mean values from four independent measurements.

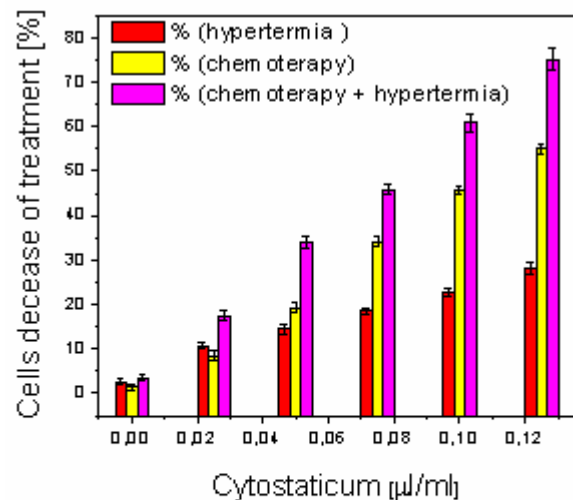


Fig.2. Dependence of tumors cells decrease percent from various concentrations of magnetic particles, Gleevec and Gleevec-magnetosomes. The results are mean values from twelve independent measurements.

Acknowledgement

This work was supported by the research grant from the Slovak grantagency Vega No. 1/2012/05.

References

- [1] M. Zahn, C. Rinaldi: Effects of spin viscosity on ferrofluid flow profiles in alternating and rotating magnetic fields, *physics of fluids*, 14 (2002) 2847-2870
- [2] I. Safarik and M Safarikova,; Magnetic Nanoparticles and Biosciences, *Mon. Chem.*, 133 (2002), 737-759
- [3] M. Babinová, V. Altanerová, Č. Altaner, P. Babinec: In vivo heating of magnetic nanoparticles in alternating magnetic field. *Medical Physics*, 31 (2004) 2219
- [4] M. Babinová, D. Leszczynska, P. Sourivong, P. Babinec, J. Leszczynski: Principles of magnetodynamic chemotherapy. *Medical hypotheses*, 62 (2004) 375-377
- [5] M. Deininger, E. Buchdunger, and B. J. Druker: The development of imatinib as a therapeutic agent for chronic myeloid leukemia *Blood*, 105 (2005) 2640 – 2653
- [6] D. M. Steinert; J. C. McAuliffe; J. C. Trent: Imatinib mesylate in the treatment of gastrointestinal stromal tumour, *Expert Options on pharmacotherapy*, 6 (2005) 105-113

Effect of Hofmeister series cations on activity and stability of NADH oxidase from *Thermus thermophilus*

K. TÓTH¹, G. ŽOLDÁK¹ AND E. SEDLÁK¹

¹Department of Biochemistry, P. J. Šafárik University, Moyzesova 11, 041 54 Košice, Slovakia.
e-mail: kamil_toth@yahoo.com

Finding of the conformational dynamic - function relationships is important topic in biochemistry that enable us intelligent design of the active state. External conditions such as various denaturants (salts, urea, guanidium hydrochloride etc.) have the ability to modulate enzyme activity: (i) directly through ion binding and adsorption (model of the site specific binding); and/or (ii) indirectly through changing solvent activity and structure (weak interaction model) [1]. This two different treatments led also to different response of the protein dynamics. In the case of the ligand binding enzyme dynamics is likely reduced or remain unchanged due to ligand occupation of the binding cavity and increase of the local atomic density. Weak interaction model treats the salt as the chemical perturbant of the solvent-solvent interaction (e.g. surface tension) and solvent-protein interaction that are directly coupled with protein dynamics. Changing of the salt concentration provide for us unique opportunity to the careful and define external tuning of the protein dynamics.

NADH oxidase (E.C.1.6.99.3) from extreme thermophilic organism *Thermus thermophilus* belongs to $\alpha+\beta$ class of proteins. This small (44.5 kDa) homodimeric flavoenzyme is member of the novel flavin oxidoreductase family. Isoelectric point of this protein is $pI \sim 9.25$. In comparison with other flavin oxidoreductases (average $pI \sim 6.2$), NADH oxidase is the most basic member of this family. One molecule FAD or FMN per monomer binds at the dimeric interface with dissociation constants of $1 \cdot 10^{-5}$ M and $9 \cdot 10^{-8}$ M, respectively [2]. NADH oxidase catalyzes the oxidation of NADH followed by the reduction of the intrinsic flavin cofactor. Depending on the *in vitro* conditions, there are two different ways of the recovery of reduced flavin cofactor: (1) in the absence of the other electron acceptor, two electron transfers reaction on oxygen molecules and formation of H_2O_2 ; and (2) electron and hydride transfer on the suitable organic electron acceptor, e.g. exogenous FMN. The later represents major reaction pathway for reduced flavin even under aerobic conditions. The physiological role of NADH oxidase from *Thermus thermophilus* is not known.

Previous studies in our laboratory give us interesting results about influence of **Hofmeister series anions** on thermophilic NADH oxidase and the conformational dynamic in the active site [3]. Both chaotropic and kosmotropic anions at high concentrations, inhibit enzyme activity. Low activity in the presence of the kosmotropic reagents may be enhanced by the addition of denaturant – urea but no increase of activity was observed in the chaotropic salts. Active site contains an excellent fluorescence marker - flavin molecule. Fluorescence quenching experiments of flavin cofactor show that high concentration of kosmotropic salts led to the decreasing of the flavin accessibility. On the other hand, chaotropic reagents led to increasing of the flavin quenching by external quenchers. Circular dichroism spectra reveal that secondary structure is not changed at high salt concentrations. Based on the experimental findings, we proposed that high rigidity of the active site in the presence of kosmotropic anions and its high flexibility in the presence of chaotropic anions have a decelerating effect on enzyme activity.

Now, our interest is focused on the **Hofmeister series cations**. Generally, cations have lower efficiency in promoting of Hofmeister effect due to asymmetry of the charge distribution in water molecule [4]. The effect of the cations on NADH oxidase activity at neutral pH may be weaker due to high pI of the NADH oxidase. Large excess of the positive

charge on the protein surface disfavours cation binding and non-specific adsorption. We used different types of cations of chloride salt. Our results show that in all studied cations (NH_4^+ , Gdm^+ , Li^+ , Na^+ , K^+ , Cs^+) activity of the enzyme is non-specifically increased about ~3 fold at 0.75-2.0 M concentration. At higher salt concentrations activity decreases as follow: $\text{Gdm}^+ < \text{Li}^+ < \text{Na}^+ \approx \text{K}^+ < \text{Cs}^+ < \text{NH}_4^+$. Dependence of enzyme activity on salt concentration is similar for Na^+ and K^+ salts in agreement with our previous findings [3]. Except guanidinium and lithium, cations have only modest ion specific effect on activity in opposite to the anion specific effect. Guanidinium and lithium significantly decrease activity, whereas ammonium chloride is a potent enzyme activator. Thermal denaturation of the enzyme was performed in order to estimate differences in protein stability. At 2 M salt concentrations transition temperatures decrease in order: $\text{Gdm}^+ \ll \text{NH}_4^+ < \text{Li}^+ < \text{Cs}^+ \approx \text{Na}^+ \approx \text{K}^+$. Strong chaotropic guanidinium cation significantly decreases transition temperature from 83 °C to 68 °C and enzyme activity is very low. In the presence of 2 M NH_4^+ cations, protein has higher transition temperature than guanidinium and highest activity of all studied salts. The rest cations have higher transition temperature but lower activity than ammonium cation. In conclusion, high transition temperature is not associated by the high enzyme activity.

Acknowledgement (Times New Roman, veľkosť 10)

This work was supported by the research grant from the Slovak Grant Agency Vega No. 1/0432/03 and 1/3252/06.

References

- [1] R. L. Baldwin, *Biophysical Journal* 71 (1996), 2056-2063.
- [2] H. J. Hecht, H. Erdmann, H. J. Park, M. Sprinzl, R. D. Schmid, *Nat.Struct.Biol.* 2 (1995), 1109-1114.
- [3] G. Žoldák, M. Sprinzl and E. Sedlák, *Eur. J. Biochem.* 271 (2004), 48-57.
- [4] K. D. Collins, *Biophysical Journal* 72 (1997), 65-76.

Stochastic simulations of photophysical processes: Applications of Dizzy to simulation of photoinduced reactions

Cs. ULIČNÁ¹ AND J. ULIČNÝ²

¹ Department of information technologies and services, University library of Prešov University, 17. November st. 1, 080 01 Prešov, Slovakia.

e-mail: ulicna@unipo.sk

² Department of Biophysics, P. J. Šafárik University, Jesenná 5, 041 54 Košice, Slovakia.

e-mail: ulicny@bioflab.upjs.sk

Even for relatively simple photochemical processes, the dynamics of photoinduced cascade of events may follow complicated path. Existence of different competing reaction channels, molecule concentration effects, particular geometry and mutual orientation of interacting molecules and light quanta density all play role in particular experimental setup. Individual competing processes may act on different time scale, which leads to rich variety of experimental observations. Computational modeling of such processes can significantly contribute to our understanding of experimentally observed dynamics and help to spot eventual inconsistencies of interpretation of experiment.

In our contribution, simple adaptation of stochastic kinetics simulation package Dizzy [1] for photophysical and photochemical applications is presented. Dizzy is molecular reaction kinetics software, written for stochastic simulations of biochemical reactions. In comparison with other modeling packages [2-6] Dizzy has impressive expressive capabilities and easy-to-learn user interface which facilitate modeling of wide range of reaction events for non-specialists. In its present state it lacks, however, some features allowing direct simulations of photoprocesses without workarounds.

Using suitable modifications of the core package, the dynamics of photoprocesses relevant to experimental observations can be modeled and monitored.

The application of this tool is demonstrated on two models, relevant to actual experiments: fluorescence correlation spectroscopy (FCS) experiments and singlet oxygen production dynamics.

Acknowledgement

This work was supported by the research grant from the Slovak Grant Agency Vega 1/1018/04.

References

- [1] S. Ramsey, D. Orrell, H. Bolouri, Dizzy: Stochastic simulation of large-scale genetic regulatory networks, *J. Bioinformatics Comput. Biol.* Vol. 3. No. 2 (2005), pp. 415-436.
- [2] C. J. Morton-Firth and D. Bray, Predicting temporal fluctuations in an intracellular signaling pathway, *J. Theor. Biol.* 192 (1998), 117-128.
- [3] J. Puchalka and A. M. Kierzek, A. M., Bridging the gap between stochastic and deterministic regimes in the kinetic simulations of the biochemical reaction networks, *Biophys. J.* 86 (2004), 1357-1372.
- [4] A. M. Kierzek, STOCKS: STOChastic Kinetic Simulations of biochemical systems with Gillespie algorithm, *BIOINFORMATICS* 18(3) (2002): 470-481.
- [5] B. M. Slepchenko, J. C. Schaff, I. Macara and L. M. Loew, Quantitative cell biology with the Virtual Cell, *Trends Cell Biol.* 13 (2003): 570 – 576.
- [6] M. Tomita, K. Hashimoto, K. Takahashi, T. Shimizu, Y. Matsuzaki, F. Miyoshi, K. Saito, S. Tanida, K. Yugi, J.C. Venter, and C. Hutchison, E-CELL: Software environment for whole cell simulation, *Bioinformatics* 15(1) (1999):72-84.

Hydrogen Cyanide Binding to Cytochrome *c*: Effect of pH, Ionic Strength and Denaturant

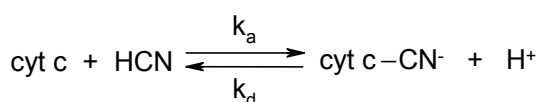
R. VARHAČ¹ AND M. ANTALÍK^{1,2}

¹ Institute of Experimental Physics SAS, Košice, Slovakia

² Department of Biochemistry, Faculty of Natural Sciences UPJŠ, Košice, Slovakia

The rate constant of HCN binding to oxidized cytochrome *c* was studied as a function of pH by means of absorption spectroscopy. The experiments were performed at constant temperature (20 °C) and pH below 7.0 in three different solution conditions: low ionic strength (5 mM phosphate or acetate buffer), high ionic strength (0.5 M NaCl) and urea (2.0 and 4.0 M). It is well known that cytochrome *c* undergoes conformational transition from native to denatured state in acidic pH [1]. During this transition the original His18–Fe–Met80 iron axial configuration changes to His18–Fe–H₂O configuration. The aim of this study was to point out that there is a direct correlation between the acid induced conformational transition of cytochrome *c* and the rate of cytochrome *c*-CN⁻ formation.

Cytochrome *c* binds HCN forming low-spin six-coordinated complex characterized by the absorption maximum at 413 nm. Generally accepted mechanism for hydrogen cyanide binding in acidic solutions assumes that HCN diffuses into the heme pocket and after dissociation to H⁺ and CN⁻ the latter binds to the heme iron [2] thus substituting for the sixth axial ligand, Met80. The simplest kinetic scheme for the complex formation is expressed by following equation:



Observed rate constant of this process, k_{obs} , can be written as a linear function of HCN concentration according to equation:

$$k_{\text{obs}} = k_d + k_a[\text{HCN}]$$

where k_d represents dissociation rate constant and k_a is association rate constant of the reaction.

Figure 1 shows the values of observed rate constants as a function of HCN concentration at pH 3.38, 2.96 and 2.33. This dependence clearly demonstrates linearity in the range from 6 to 40 mM HCN in all three cases. As the concentration of the ligand increases, up-shift (pH 3.38) or down-shift (pH 2.33) curvature can be observed. It should be noted that the solution of HCN contains equivalent amount of Cl⁻ ions originating from hydrochloric acid used to adjust pH of the initial KCN solution ($pK_{\text{HCN}} = 9.25$ at 22 °C). This finding gives an evidence for the salt effect on the k_{obs} and thus k_a value that represents the slope of the above dependence. The plot of k_a versus pH in low ionic strength is shown in Figure 2a (only k_{obs} in the range from 0 to 40 mM HCN were taken into account to minimize the effect of Cl⁻ ions). The k_a values determined in 0.5 M NaCl are also shown and as can be seen, pH of the maximal k_a ($k_{a,\text{max}}$) is slightly shifted to higher values as compared to a solu-

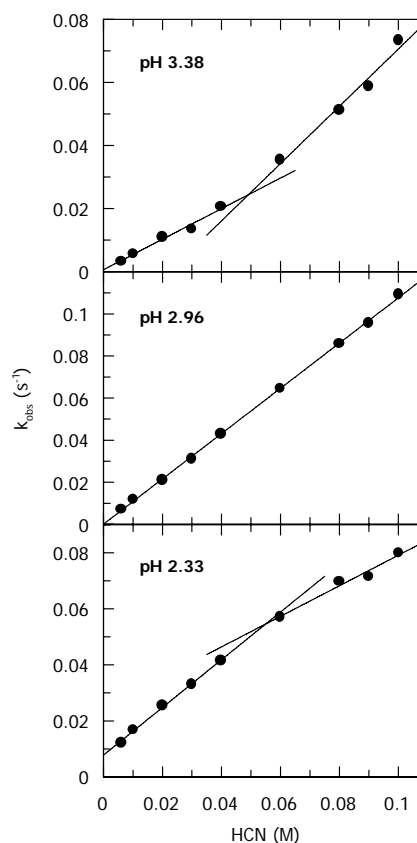


Fig. 1 Dependence of the observed pseudo-first-order rate constants on HCN concentration for the interaction of HCN with cytochrome *c* at three different pH values, 5 mM phosphate buffer, 20 °C.

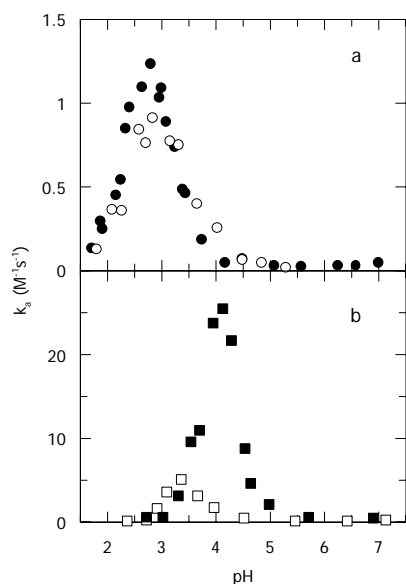


Fig. 2 pH dependence of the association rate constant, k_a , for cytochrome *c*-CN⁻ complex formation in (a) 5 mM phosphate or acetate buffer (solid circles) and 0.5 M NaCl (open circles), and in (b) 2.0 M urea (open squares) and 4.0 M urea (solid squares), 20 °C.

as an obstruction in cyanide ligation which makes the association rate constant lower.

Up to now, to study accessibility of the metal's sixth coordination position in heme proteins low-molecular ligands such as HCN were applied in the pH range where the protein remained folded. We have shown that they can be also used to monitor some specific features relevant to the process of protein unfolding.

Acknowledgement

This work was supported by the research grant from the Slovak Grant Agency Vega No. 4068 and 6167.

References

- [1] H. Theorell and Å. Åkesson, *J. Am. Chem. Soc.* 63 (1941), 1812-1818.
- [2] P. George and C. L. Tsou, *Biochem. J.* 50 (1952), 440-448.
- [3] R. Varhač and M. Antalík, *Biochemistry* 43 (2004), 3564-3569.
- [4] Y. P. Myer and A. F. Saturno, *J. Protein Chem.* 10 (1991), 481-494.
- [5] R. Varhač, *PhD. Thesis* (2005), University of P. J. Šafárik, Košice.
- [6] S. Oellerich, H. Wackerbarth and P. Hildebrandt, *J. Phys. Chem. B* 106 (2002), 6566-6580.

tion of low ionic strength. Also evident is a drop in the absolute value of $k_{a,max}$ by about $0.3 \text{ M}^{-1}\text{s}^{-1}$ in the case of 0.5 M NaCl. Contrary to NaCl that stabilizes protein secondary structure, application of denaturant such as urea causes its destabilization. This results in a strong increase of k_a values as well as in a shift of $k_{a,max}$ to neutral pH in the presence of 2.0 and 4.0 M urea (Figure 2b). The common feature of all mentioned dependences is the bell-like shape and the close resemblance of their pH value of $k_{a,max}$ with corresponding pK value determined by acid-induced denaturation of cytochrome *c* at 695 nm (see Table 1). This result can be explained in term of cytochrome *c* denaturation that is characterized by the gradual opening of the heme crevice and simultaneous dissociation of the Fe-S(Met80) coordination bond. So the initial increase of the k_a values as pH decreases is in accordance with this scheme. More surprising are the decreasing limbs of the k_a versus pH plots. This behavior can be the most probably attributed to the existence of a heme coordinated competitive ligand that was found to be water in the acidic pH in and without the presence of urea [6]. Water coordination can act

Table 1 Comparison of cytochrome *c* pK_{695nm} values at different solution conditions with corresponding pH of $k_{a,max}$ for HCN binding to cytochrome *c*

solution conditions	pH ($k_{a,max}$)	pK_{695nm}	ref.
5 mM phosphate	2.80	2.62	[3]
0.5 M NaCl	2.84	2.90 ^a	[4]
2.0 M urea	3.36	3.46	[5]
4.0 M urea	4.13	4.13 ^b	[5]

^a Measured in 0.2 M KCl. ^b Determined in 3.9 M urea.

Conformation and heme configuration of ferricytochrome *c* in the presence of sorbitol and NaCl at pH 2 and 3.2.

J. BÁGEL'OVÁ¹, D. FEDUNOVÁ¹, Z. GAŽOVÁ¹ AND M. ANTALÍK^{1,2}

¹ Department of Biophysics, Institute of Experimental Physics, SAS, Košice, Slovakia.

² Department of Biochemistry, Faculty of Natural Sciences, P. J. Šafárik University, Košice, Slovakia.

e-mail: fedunova@saske.sk

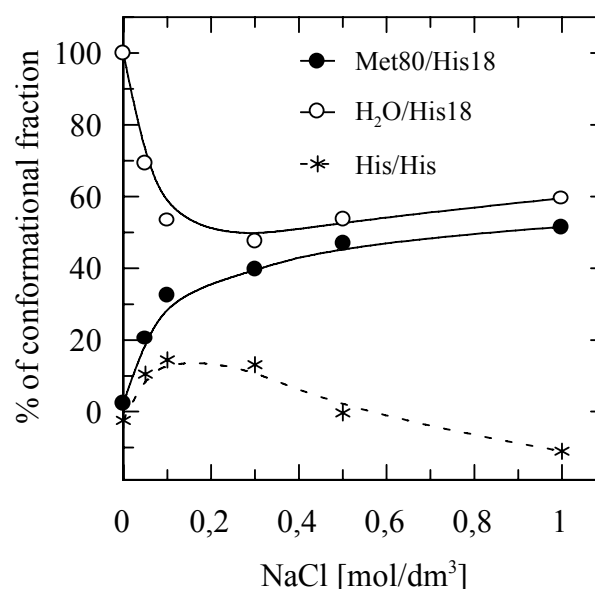
It is well known that cytochrome *c* (cyt *c*) exists in different, stable conformational states having altered heme ligation under various pH- and salt-dependent conditions. Native state of cyt *c* contains three major helices and two minor helical elements interconnected by loops, and its heme (covalently bound to Cys 14 and Cys 17) is axially ligated with His 18 and Met 80 to yield a six-coordinated low spin form. It was observed that the viscosity of cyt *c* at low ionic strength increased from 2.6 cm³/g at neutral pH to 22.5 cm³/g at pH 2, at 25°C, indicating that the peptide chain undergoes a transition from the native state globular form to an extended random configuration at low pH and cyt *c* probably loses an axial heme ligand.

Upon increasing the ionic strength (0.5M NaCl) and low pH, a compact equilibrium state of cyt *c* is re-formed. It has native-like secondary structure (helical) but is loosely folded, lacking a stable tertiary structure, which is called the molten globule (MG) state [1].

To understand the principles of protein stability it is important to elucidate the stabilizing mechanisms of native state as well as MG state, an intermediate between native and denatured states. A significant influence of salts or charges on the stability of cyt *c* molten globule (MG) state revealed that main driving force of MG state is reduction of the electrostatic repulsion between charged residues, which favors the unfolded conformations [2]. Addition of NaCl reduces the electrostatic repulsion but has only small effects on the hydrogen bond and hydrophobic interaction at low concentration, producing the net force favorable for MG formation.

It has been reported that polyols or alcohols induce the MG state of cyt *c*. Driving force for this process increased steric repulsion between the proteins and solution. Santucci et al. [3] has reported the formation of molten globule like state of cytochrome *c* induced in the presence of high concentration of glycerol. From two native axial ligands of the heme iron, only His 18 is thought to remain coordinated to the heme iron in this state while the Met 80 axial bond is lost.

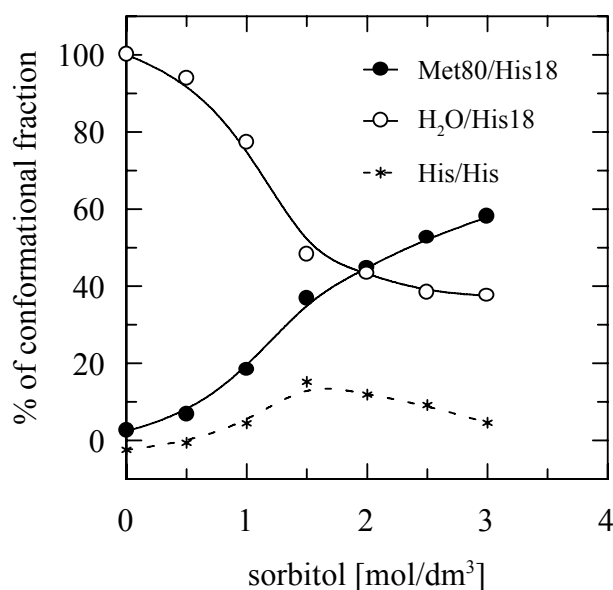
Polyols have only small effects on the electrostatic interaction because the dielectric constant of water is not so markedly reduced to bring about the ion-pair formation even at high sorbitol concentration. A dominant solvent effect of sorbitol is stabilization of hydrophobic interaction [4].



The dependence of individual conformational fractions of cyt *c* molecules with different heme-iron ligands on NaCl concentration at pH 2, 25°C.

The bond Met80-heme iron is one of the most sensitive parts of ferricytochrome c molecule to disorder by increasing temperature or changing pH. The 695 nm absorption band is a feature directly linked to the presence or absence of the Met80-heme iron linkage.

We have investigated the effects of various concentrations of sorbitol and NaCl on the



The dependence of individual conformational fractions of cyt c molecules with different heme-iron ligands on sorbitol concentration at pH 2, 25°C.

stability of the axial ligands of cyt c in acidic pH region. Addition of 1M NaCl significantly changes the apparent pK value of conformation change at heme region of cyt c. It changes from 2.5 to 3.5. 3M sorbitol shifts pK value only slightly, to pK equal ~ 2.2.

We observed that MG state of cyt c induced by 1M NaCl (pH2, 25°C), involves 50% cyt c molecules with native axial ligands. Similarly, 3M sorbitol (pH2, 25°C) induce native heme coordination at 60% cyt c molecules.

Different behaviour is observed at pH 3.2. While 1M NaCl decrease the fraction of cyt c molecules containing the Met80-heme iron bond to 70%, 3M sorbitol does not change the heme ligands.

The midpoint of the thermal transition of cyt c with 1M NaCl or 3M sorbitol (pH

3.2) was found at 40.8 °C and 68.5°C, respectively (cyt c = 58.5°C). The equilibrium between ligands is very dependent on temperature. Low temperatures favor Met80/His18 configuration and high temperatures H₂O/His configuration of cyt c heme iron.

Acknowledgement

This work was supported by the research grants from the Slovak Grant Agency Vega No. 4068 and 6167.

References

- [1] Y. Goto, Y. Hagihara, D. Hamada, M. Hoshino and I. Nishii, *Biochemistry* 32 (1993) 11878-11885.
- [2] Y. Goto and A.L. Fink, *Biochemistry* 28 (1989), 945-952.
- [3] R. Santucci, C. Bongiovanni, G. Mei, T.P. Ferri, F. Polizio and A. Desideri, *Biochemistry* 39 (2000), 12632-12638.
- [4] T. Kamaiyama, Y. Sadahide, Y. Nogusa and K. Gekko, *Biochim.Biophys. Acta* 1434 (1999), 44-57.

A faint, light blue abstract graphic consisting of several curved, overlapping lines that form a stylized, organic shape, possibly resembling a flower or a leaf. It is centered in the background of the page.

LIST OF PARTICIPANTS

ŠTEFAN BÁLINT

Department of Biophysics, Institute of Physics, Faculty of Science, P.J. Šafárik University, Košice
balint.stefan@gmail.com

MICHAL CAGALINEC

International Laser Centre, Bratislava
Bratislava
misoc@ilc.sk

DUŠAN CHORVÁT

International Laser Centre, Bratislava
chorvat@ilc.sk

DUŠAN CHORVÁT, JR.

International Laser Centre, Bratislava
dusan@ilc.sk

ROMAN DURNÝ

Department of Biophysics, Institute of Physics, Faculty of Science, P.J. Šafárik University, Košice
dikinovic@yahoo.com

GABRIELA FABRICOVÁ

Department of Biophysics, Institute of Physics, Faculty of Science, P.J. Šafárik University, Košice
gfabrici@seneca.science.upjs.sk

DIANA FEDUNOVÁ

Department of Biophysics, Institute of Experimental Physics, Slovak Academy of Sciences, Košice
fedunova@saske.sk

ZUZANA GAŽOVÁ

Department of Biophysics, Institute of Experimental Physics, Slovak Academy of Sciences, Košice
gazova@saske.sk

PETER GBUR

Department of Biophysics, Institute of Physics, Faculty of Science, P.J. Šafárik University, Košice
gbenik@gmail.com

VALÉRIA HAVRILOVÁ

Department of Biophysics, Institute of Physics, Faculty of Science, P.J. Šafárik University, Košice
havrilv@kosice.upjs.sk

TIBOR HIANIK

Department of Nuclear physics and Biophysics, Faculty of Mathematics, Physics and Informatics,
Comenius University, Bratislava
hianik@fmph.uniba.sk

DANIEL JANCURA

Department of Biophysics, Institute of Physics, Faculty of Science, P.J. Šafárik University, Košice
djancura@yahoo.com

JANA KIRCHNEROVÁ

Faculty of Mathematics, Physics and Informatics, Comenius University, Bratislava
kirchnerova@ilc.sk

LIST OF PARTICIPANTS

GEJZA LAJOŠ

Department of Biophysics, Institute of Physics, Faculty of Science, P.J. Šafárik University, Košice
new180@gmail.com

PAVOL MIŠKOVSKÝ

Department of Biophysics, Institute of Physics, Faculty of Science, P.J. Šafárik University, Košice
misko@kosice.upjs.sk

PETER MURÍN

Institute of Medical Biophysics, Comenius University, Jessenius Faculty of Medicine, Martin
pmurin@jfmmed.uniba.sk

ZUZANA NAĐOVÁ

Department of Biophysics, Institute of Physics, Faculty of Science, P.J. Šafárik University, Košice
znadova@centrum.cz

PAVEL NOVÁK

Institute of Molecular Physiology and Genetics, Slovak Academy of Sciences, Bratislava
pavel.novak@savba.sk

JARMILA PODSKOČOVÁ

Faculty of Mathematics Physics and Informatics, Comenius University, Bratislava
podskocova@ilc.sk

DANICA SABOLOVÁ

Department of Biochemistry, Institute of Chemistry, P. J. Šafárik University, Košice
sabdan@kosice.upjs.sk

MARTIN SAVKO

Department of Biophysics, Institute of Physics, Faculty of Science, P.J. Šafárik University, Košice
martin.savko@post.sk

KRISTÍNA SCHRNEROVÁ

Department of Nuclear physics and Biophysics, Faculty of Mathematics, Physics and Informatics,
Comenius University, Bratislava
schrnerova@fmph.uniba.sk.sk

ERIK SEDLÁK

Department of Biochemistry, Institute of Chemistry, Faculty of Science, P. J. Šafárik University,
Košice
sedlak_er@yahoo.com

JOZEF SMOLKA

International Laser Centre, Bratislava
smolka@ilc.sk

JANA STANIČOVÁ

Department of Chemistry, Biology and Biochemistry, University of Veterinary Medicine, Košice
stanicova@uvm.sk

BARBORA TENCEROVÁ

Department of Nuclear physics and Biophysics, Faculty of Mathematics, Physics and Informatics,
Comenius University, Bratislava
b.tencerova@centrum.sk

KAMIL TÓTH

Department of Biochemistry, Institute of Chemistry, Faculty of Science, P. J. Šafárik University,
Košice
kamil_toth@yahoo.com

CSILLA ULIČNÁ

Department of information technologies and services, University library of Prešov University, Prešov
ulicna@unipo.sk

JOZEF ULIČNÝ

Department of Biophysics, Institute of Physics, Faculty of Science, P.J. Šafárik University, Košice
ulicny@seneca.science.upjs.sk

RASTISLAV VARHAČ

Department of Biophysics, Institute of Experimental Physics, Slovak Academy of Sciences, Košice
varhac@saske.sk

PAVOL VITVIČ

Department of Nuclear physics and Biophysics, Faculty of Mathematics, Physics and Informatics,
Comenius University, Bratislava
palino1978@yahoo.com

IVAN ZAHRADNÍK

Institute of Molecular Physiology and Genetics, Slovak Academy of Sciences, Bratislava
ivan.zahradnik@savba.sk

ALEXANDRA ZAHRADNÍKOVÁ

Institute of Molecular Physiology and Genetics, Slovak Academy of Sciences, Bratislava
alexandra.zahradnikova@savba.sk



**AUTHOR
INDEX**

Adamčík J.	52	Kubalová Z.	20
Antalík M.	24, 48, 50, 69, 71	Kurča E.	17
Babincová M.	62, 64	Lacík I.	39
Bágeľová J.	48, 50, 71	Lajoš G.	55
Bálint Š.	45, 55	Mateášik A.	41, 43, 53
Bánó M.	48	Maurizot J. C.	53
Berka V.	24	Miškovský P.	26, 45, 52, 53, 55
Bíró Cs.	55	Mĺkvy P.	43
Burianková L.	45	Muriň P.	17
Cagalinec M.	29, 41	Novák P.	22
Chorvát D., Jr.	29, 39, 41, 52	Palmer G.	24
Chorvátová A.	29, 41	Podhradský D.	56
Danko P.	52	Podskočová J.	39
Dědic R.	26	Pavelková J.	20
Dobbek H.	33	Poláková E.	20
Durný R.	47	Refregiers M.	52, 53
Fabián M.	24	Sabolová D.	56
Fabriciová G.	45, 52	Sabová J.	56
Fedunová D.	48	Savko M.	27, 58
Gažová Z.	50, 71	Schronerová K.	62
Gbur P.	26	Sedlák E.	33, 35, 37, 60, 66
Grillenbeck N.	33	Sedláková D.	60
Grman I.	15	Smolka J.	43
Hála J.	26	Sprinzl M.	33
Havrilová V.	52	Tencerová B.	64
Hianik T.	15, 31	Thompson T.	15
Hritz J.	37	Tomášková N.	60
Huntošová V.	53	Tóth K.	35, 66
Jakuš J.	17	Uličná Cs.	68
Jancura D.	24, 26, 45, 52, 53, 58	Uličný J.	27, 47, 58, 68
Kaščáková S.	26, 53, 58	Varhač R.	60, 69
Kirchnerová J.	29	Varinská L.	60
Kolláriková G.	39	Vitovič P.	31
Kožurková M.	56		

AUTHOR INDEX

Vörtler S. 33

Zahradníková A., Jr. 20

Zahradník I. 18, 20, 22

Žoldák G. 33, 35, 37, 60, 66

Zahradníková A. 18, 20